

Kronian Magnetospheric Reconnection Statistics Across Cassini's Lifetime

T. M. Garton^{1,*}, C. M. Jackman², A. W. Smith³

¹Space Environment Physics Group, Department of Physics and Astronomy, University of Southampton,
Southampton, England

²School of Cosmic Physics, DIAS Dunsink Observatory, Dublin Institute for Advanced Studies, Dublin 15,
Ireland

³Mullard Space Science Laboratory, Department of Space and Climate Physics, University College
London, London, England

Key Points:

- Machine learning classifications in previously unobserved environments can be validated through iterative runs.
- The Cassini data do not reveal a quasi-steady magnetotail reconnection x-line inside of $< 70 R_S$.
- Cassini observations indicate a mass loss rate of $\sim 34.4 \text{ kg s}^{-1}$ due to magnetotail plasmoid release.

Corresponding author: Tadhg Garton, t.m.garton@soton.ac.uk

Abstract

Magnetic reconnection is a fundamental physical process in planetary magnetospheres, in which plasma can be exchanged between the solar wind and a planetary magnetosphere, and material can be disconnected and ultimately lost from a magnetosphere. Magnetic reconnection in a planetary magnetotail can result in the release of plasmoids downtail and dipolarizations planetward of an x-line. The signatures of these products include characteristic deflections in the north-south component of the magnetic field which can be detected by in-situ spacecraft. These signatures have been identified by eye, semi-automated algorithms, and recently machine learning methods. Here, we apply statistical analysis to the most thorough catalogue of Kronian magnetospheric reconnection signatures created through machine learning methods to improve understanding of magnetospheric evolution. This research concludes that no quasi-steady position of the magnetotail x-line exists within 70 R_S . This research introduces prediction equations to estimate the distribution of duration of plasmoid passage over the spacecraft ($N = 300\Delta t^{-1.3}$, bin width = 1 min) and north-south field deflection ($N = 52\Delta B_\theta^{-2.1}$, bin width = 0.25 nT) expected to be identified by an orbiting spacecraft across a year of observations. Furthermore, this research finds a local time asymmetry for reconnection identifications, with a preference for dusk-side over dawn-side. This may indicate a preference for Vasyliunas style reconnection over Dungey style for Saturn. Finally, through these distributions, the reconnection rate of Saturn's magnetotail can be estimated as 3.22 reconnection events per day, with a resulting maximum mass loss from plasmoids of 34.4 kg s^{-1} on average, which is comparable with the magnetospheric mass loading from Enceladus ($8\text{-}250 \text{ kg s}^{-1}$).

1 Introduction

Magnetic reconnection is the process whereby a magnetic field enters a state of stress or strain and restructures itself into a lower energy state (Hesse & Cassak, 2020). This often occurs through the explosive snapping and reforging of magnetic field lines, creating a release of energy and mass as byproducts. For planets with well-developed magnetospheres, reconnection between the interplanetary magnetic field and planetary magnetic field on the day-side of a magnetosphere can result in the transfer of energy, mass and momentum (Milan et al., 2007; McAndrews et al., 2008). Similarly, on the night-side, open magnetic field lines become stretched into a extended planetary magnetotail which facilitates reconnection to again form closed field lines (Dungey, 1961; Dungey, 1965). This cyclic transition between open and closed field configurations allows the transfer of mass and energy, both in and out, of the planetary magnetosphere, as well as alters the ratio of open-closed magnetic flux to the magnetosphere. Alternatively, reconnection can occur for rapidly rotating magnetized planets, such as Saturn, which involves no variation in overall magnetic flux. For these planets rapid rotation rates and significant internal mass sources result in the operation of the Vasyliunas cycle where mass is lost down the magnetotail through the reconnection of centrifugally stretched, mass loaded field lines (Vasyliunas, 1983).

Figure 1 illustrates a model of night-side magnetospheric reconnection occurring within the planetary current sheet. Direct encounters with the reconnection site are extremely rare: at Saturn there has been one reported observation of the ion diffusion region (Arridge et al., 2015). The vast majority of reconnection-related knowledge has been derived from in situ encounters with the products of reconnection: plasmoids, travelling compression regions and dipolarizations, all of which leave characteristic signatures in field and particle data. On the planet-side of the reconnection site reconnection can be identified indirectly by spacecraft through dipolarizations, when the north-south magnetic field undergoes a negative to positive deflection caused by a contracting of reconnected magnetic field back towards the planet (Bunce et al., 2005; Russell et al., 2008; Jackman et al., 2013, 2015; Yao et al., 2017; Smith et al., 2018a, 2018b). On the tail-side, reconnection can be remotely identified through plasmoids (Hones, 1977; Richard-

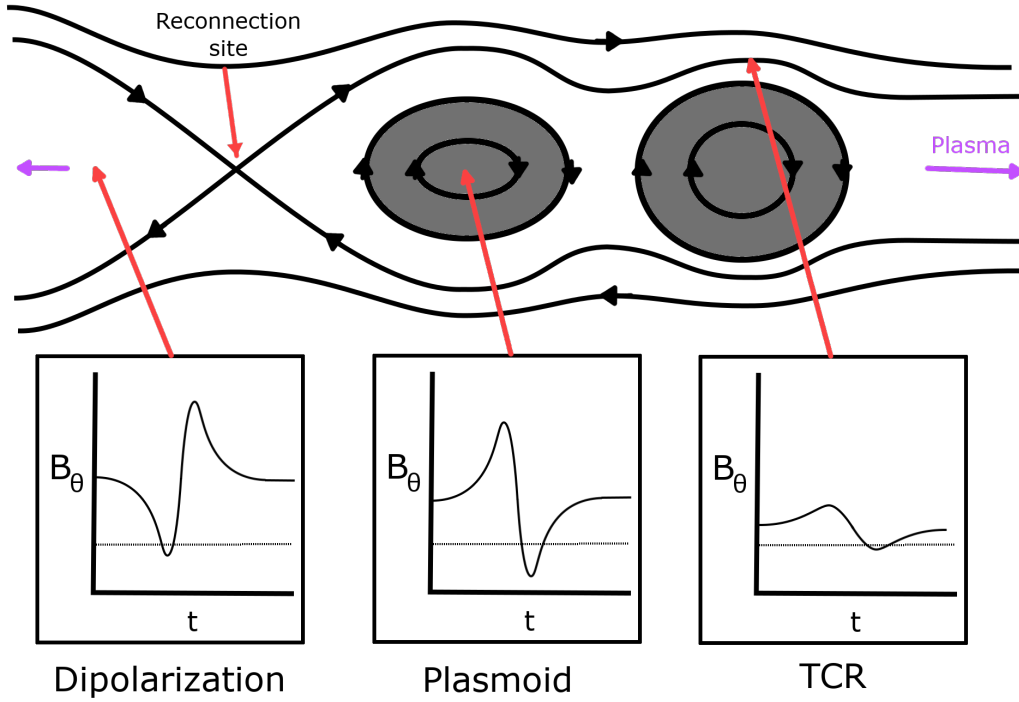


Figure 1. Model of magnetic reconnection in a planetary current sheet. From this form of reconnection, various structures are created: dipolarizations, plasmoids and TCRs which are detectable by in-situ spacecraft through their unique magnetic deflections (adapted from Garton et al. (2021)).

son et al., 1987; Jackman et al., 2007; Hill et al., 2008; Jackman et al., 2011a) or travelling compression regions (TCRs ; Slavin et al. (1984)), when the north-south magnetic field undergoes a severe or moderate positive to negative deflection. This is caused by either a plasmoid, enclosed bubble of magnetized plasma, or TCR, compressed bulge in the current sheet, travelling over the observing spacecraft. All of these signatures imply the bulk motion of plasma and hence, the transport of both energy and mass about the magnetosphere. Analysis on the transport of mass focuses on solving the mass budget for Saturn's magnetosphere. Saturn receives a mass loading of plasma from Enceladus of $8\text{--}250 \text{ kg s}^{-1}$ (Jurac & Richardson, 2005; Pontius Jr. & Hill, 2009; Chen et al., 2010; Fleshman et al., 2010). The MHD simulation of Zieger et al. (2010) estimated that plasmoids account for 8% of the total mass lost down-tail. Bagenal and Delamere (2011) estimated that 200 plasmoids per day would be required to remove 100 kg s^{-1} by assuming a plasmoid of volume $(10 R_S)^3$ with a density of 0.01 cm^{-3} of 18 atomic mass units (amu) ions. Jackman et al. (2014) instead estimated a distribution of 3.6-196 tail-width plasmoids per day to remove 100 kg s^{-1} with a density of 0.1 cm^{-3} of 16 amu ions (Thomsen et al., 2014).

Numerous studies have been performed on magnetospheric phenomena to understand the global impact of reconnection, ranging from changing plasma flow patterns, to dynamic auroral emissions in UV and radio wavelengths. Plasma flow patterns have been analyzed to understand the difference that reconnection makes to the pattern of sub-corotational, azimuthally-directed flow, and have been used to search for evidence

of an x-line, where one might expect oppositely directed flows on either side (McAndrews et al., 2009; Imber et al., 2011; Thomsen et al., 2014; Neupane et al., 2019). It is noteworthy that the search for Saturn’s planetary x-line has not yet been conclusive on a specific location. In addition to in-situ plasma and energetic particle investigations, remote sensing of auroral emissions in multiple wavelengths can give global context to the impact of reconnection. On the radio side, Saturn Kilometric Radiation (SKR) has been observed to both intensify and extend to lower frequencies in response to solar wind compression and magnetotail reconnection events (Jackman et al., 2009; Reed et al., 2018). Furthermore, Saturn’s UV aurora, formed at the boundary between open and closed field lines, can act as a diagnostic of the flux content of the magnetosphere, with the oval latitude changing in direct response to opening and closing of flux through reconnection (Badman et al., 2016; Bader et al., 2019; Jasinski et al., 2019). To date, these phenomena have been investigated primarily through case study observations or semi-automatically made catalogues (Bunce et al., 2005; Jackman et al., 2007; Jackman et al., 2008; Hill et al., 2008; Smith et al., 2016). However, the power of machine learning (ML) is that it enables us to explore these phenomena over wider timescales, with larger catalogues of events, and by reducing the bias associated with by-eye selection of events.

The implementation of ML to space physics is a relatively new concept, but a promising one for the improvements to identification, classification and forecasting in the field (Azari et al., 2020). ML’s strength is three-fold: its robust unbiased results, its rapid turn around from input to output, and it does not assume or require a specific analytical form or magnetic signature (Smith et al., 2017; Huang et al., 2018). ML operates through the training of a base architecture with a prepared dataset. The prepared dataset will be composed of a set of input properties and a corresponding output classification or property. The weights and biases of the base structure are gradually tuned until for the given training inputs it returns outputs with a reasonable accuracy to the expected results. This can result in over-training, where the ML model has become highly specialized to identify the training inputs with incredible accuracy, but has not learned the true underlying structure that the creator wishes to identify. To curtail this problem, the ML models are compared against new, already classified datasets in a test/validation environment. The accuracy achieved in this test environment represents the model’s true ability to classify input datasets to correct outputs (Lapedes & Farber, 1987; Jabbar & Khan, 2015; Ying, 2019). The result is a model that is efficient and accurate at identifying correct outputs for given input data. Furthermore this model is consistent: for the given input the model will always return the same output. This is contrasted with human observers, who are highly subject to unquantifiable mis-classifications, uncertainty, and bias. For a single event, two human observers may class it differently, or even the same human observer will classify datasets differently on different passes through a dataset, including being biased by the order in which data are examined. ML models are also extremely rapid with their classifications, completing potentially millions of classifications per second, far outperforming a human classifier, allowing scientific exploitation of a greater volume of data.

Garton et al. (2021) (G21) applied neural network ML methods to Cassini magnetometer data, utilizing the Smith et al. (2016) (S16) catalogue as a training set, to create a Kronian magnetospheric reconnection classifier. The S16 catalogue was created from a semi-automated classification algorithm to identify magnetotail signals of reconnection in Cassini magnetometer data through quadratic fitting and parametric thresholding. The G21 model then classified the entirety of Cassini’s near Saturn lifetime (2004–2017; see Figure 2) rendering the most complete database of magnetic field deflections. This catalogue contains start and end times of identified reconnection events, the spatial location of detection, as well as parametric information, such as the magnitude of the deflection of the north-south field component (ΔB_θ) and signal to noise ratio of the observed event. Here, we apply statistical analysis to G21 to further understanding of Saturn’s magnetic topology and its seasonal evolution, as well as introduce statistical

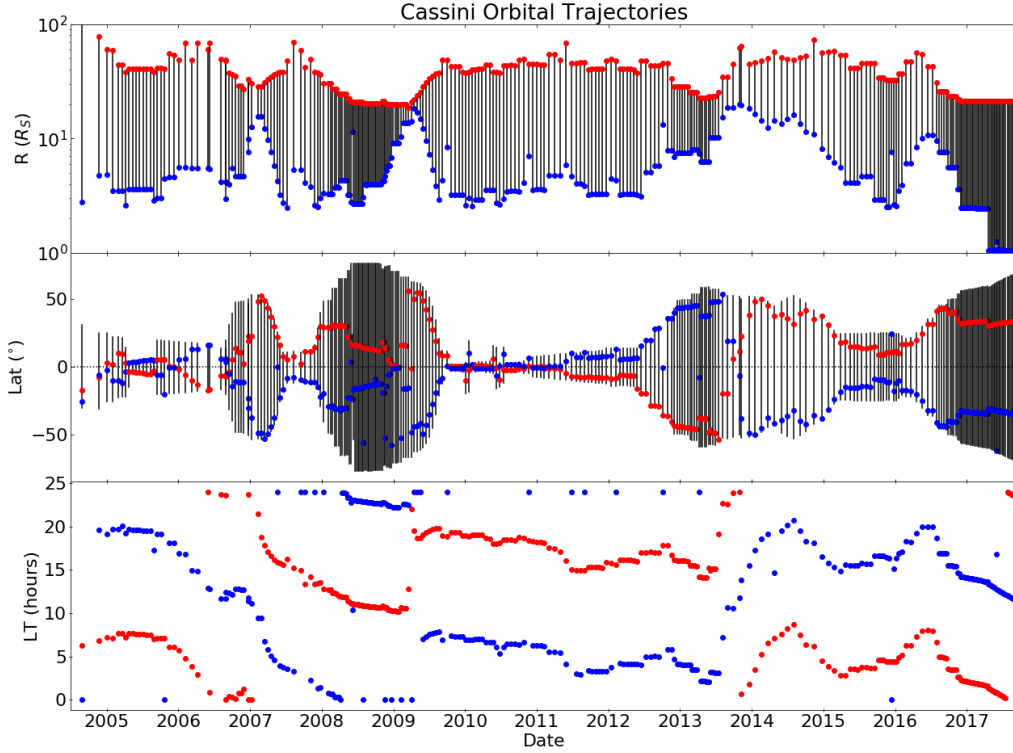


Figure 2. Trajectory of Cassini spacecraft from Saturn Orbit Insertion (July 2004) to mission end (September 2017) described in terms of its variation in radius, latitude, and local time for each orbit. Red points indicate the location of the spacecraft at apoapsis, and blue points indicate location at periapsis.

predictability to magnetospheric reconnection events. Section 2 describes catalogue validation and data pruning applied to the G21 catalogue to ensure statistical analysis is only performed on validated magnetotail events. Section 3 shows a statistical analysis across temporal, spatial, and parametric properties of validated reconnection identifications. Finally, Section 4 investigates the results of this statistical analysis and discusses the improvements to understanding of magnetospheric dynamics.

2 Catalogue Stability and Reliability

Machine learning is the next step in improvements of identification and forecasting of events in the scientific sector. However, this new method introduces unforeseen errors and complications, most notably the difficulty on interpreting machine learning architectures. This difficulty of interpretation is not due to a 'black-box'-like nature, but due to the sheer complexity and size of the architectures. While not uninterpretable, an investigation of the architecture is extremely time consuming and hence undermines the principle strength of ML methods, to save time on identification. It is important to distinguish that while these algorithms are poor at interpreting the why of events, i.e. searching for deeper meaning behind datasets, they have been shown to be extremely effective at interpreting the what, i.e. identifying positive events within a dataset on par with or outperforming human classifiers (He et al., 2015; Geirhos et al., 2018). This is why domain knowledge is critical, to marry the computation power of an ML algorithm with the domain expertise for interpretation of the scientific context. Similarly issues of sta-

bility are introduced when utilizing ML methods. Machine learning is defined by user set hyper parameters and a random starting configuration which is then fine tuned through successive epochs of training into an effective classifier. Hence, successive runs of a machine learning algorithm can produce varying results, even when using the same hyper parameters, due to the random starting positions of weights and biases, the method of separating train/test datasets, and limitations of epochs of training.

Stability for ML algorithms is typically assessed through a validation of the produced results. Metrics of accuracy and various skill scores are used to indicate an algorithm's performance on a validation or test dataset, a classified dataset which has never been seen by the algorithm during training. This is typically extremely effective at indicating an algorithm's performance and more than justifies its use when extrapolated to larger datasets. However, in space physics we typically operate in less controlled environments, with rare phenomena resulting in class imbalances and a wealth of spatial and temporal variability, hence when an algorithm is shown to be effective on a classified subset, it is not indicative of its performance on a larger unclassified dataset that experiences more varied background environments (Schneider et al., 2020). The ML algorithm constructed in G21 was trained, tested and validated on the S16 catalogue which only covers dates from the years 2006, 2009, and 2010. These years are during the optimal Cassini orbits for detecting and identifying magnetotail reconnection bi-products. Extrapolating the catalogue from these years to more varied orbits allows for the identification of more events, however these events cannot be automatically verified. Instead, we can validate these detections by comparing how consistently they are identified for each consecutive run of the ML algorithm. Figure 3 compares the distributions of ΔB_θ across 5 consecutive runs of the G21 model (same hyperparameters, such as number of hidden layers, and nodes, etc., but with variations on the training/test/validation set selection). The probability of variance in these plots describe the fractional number of minutes in events that are identified by one run of the model and not the other in 0.25 nT bins. Notably, >1 nT probability of variance reaches a plateau of ~ 0.1 across all comparisons. This indicates that 10% of detections are likely to vary between runs of the ML model. Similarly, low ΔB_θ events (<0.5 nT) reach a higher variance of ~ 0.5 . This indicates that while these detections may represent correctly identified reconnection products, they can't be consistently identified and hence should be excluded from statistical examination.

Determining an optimal threshold, above which we consider events to be validated, is difficult as, while the overall shape of distributions are similar, small scale structure in these distributions have some variation in each run comparison. To remove these local topological variations the distributions of all comparison (excluding comparisons of individual runs with themselves) can be averaged to obtain Figure 4. This figure displays average variability distributions across three parameters observed for each event in the G21 catalogue, namely (a) ΔB_θ , (b) Δt , and (c) Signal to noise ratio. These signal to noise ratio values are calculated in G21 as:

$$SNR = \frac{|\Delta B_\theta|}{B_\theta^{RMS}} \quad (1)$$

where B_θ^{RMS} is the average for a period extending 30 min either side of the central time of the event, originally sourced from S16. The distributions shown in these plots are similar to one another with a high level of variance for low values which eventually plateau at ~ 0.1 variance. A threshold of < 0.15 variance is selected as a reasonable confidence interval, below which an event is considered validated. This renders three parametric thresholds of $\Delta B_\theta = 0.71$ nT, $\Delta t = 6.61$ min, and $SNR = 1.15$. Events with all parameters above these thresholds are considered to be validated events and will be used to identify statistical trends in reconnection events. The G21 ML algorithm and associated catalogue are publically available at Garton (2020)

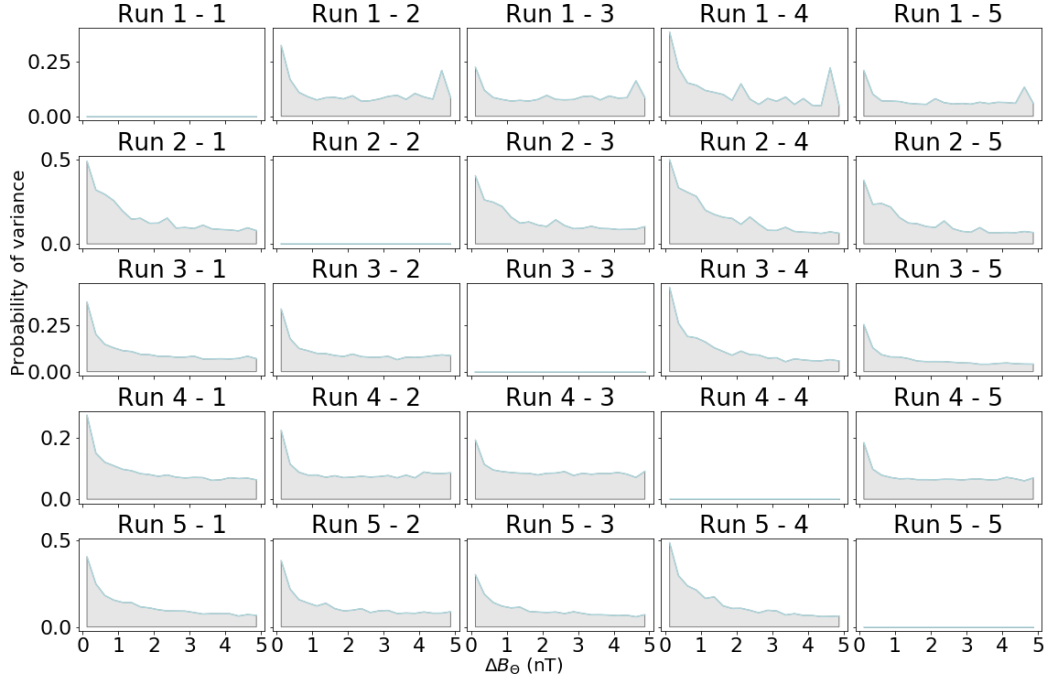


Figure 3. Minute-wise comparison of event identification stability with respect to ΔB_θ for five reconnection catalogues created through consecutive runs of the G21 neural network classification algorithm. The probability of variance indicates the fractional variation of identifications between two runs in a given 0.25 nT ΔB_θ bin.

3 Results

The ML approach is trained to identify magnetic field deflections like those in the training set. This means that bipolar deflections can be selected at any point along the Cassini trajectory (see Figure 2): not just confined to the magnetotail, but including the dayside, as well as even during magnetosheath or solar wind excursions. Figure 5 indicates the number of events identified by the ML algorithm while the Cassini spacecraft was located in the solar wind (dark blue), magnetosheath (light blue), the day-side magnetosphere (light salmon) and the night-side magnetosphere (dark salmon) for all identifications in the catalogue. These magnetic environment classifications are obtained from the Jackman et al. (2019) catalogue of magnetopause and bow shock crossings. Each of the bars in the graph are shaded with the number of events in each region that are above the three limitations set in Figure 4: 1111 solar wind, 9558 magnetosheath, 4128 day-side, and 3472 night-side events respectively. Since this catalogue is constructed from a ML method built upon the S16 catalogue, it is believed that the 3472 events within the night-side magnetosphere are considered confirmed as they represent identifications in a similar environment and under the same magnetic conditions as the catalogue the ML algorithm learned from. This does not indicate that the detections outside of the aforementioned limitations, or outside of the magnetosphere are not true identifications of signatures of reconnection, merely that they cannot be substantially validated. Signals of reconnection have been identified previously in the magnetosheath (Huddleston et al., 1997; Badman et al., 2013), on the magnetopause (Jasinski et al., 2016, 2021), and on the day-side magnetosphere (Delamere et al., 2015; Guo et al., 2018), however the underlying physical mechanisms and magnetic field morphologies which may lead to these bipolar deflections are different. On the nightside, the physical picture developed in the

Mean variability of reconnection events across the 5 ML runs

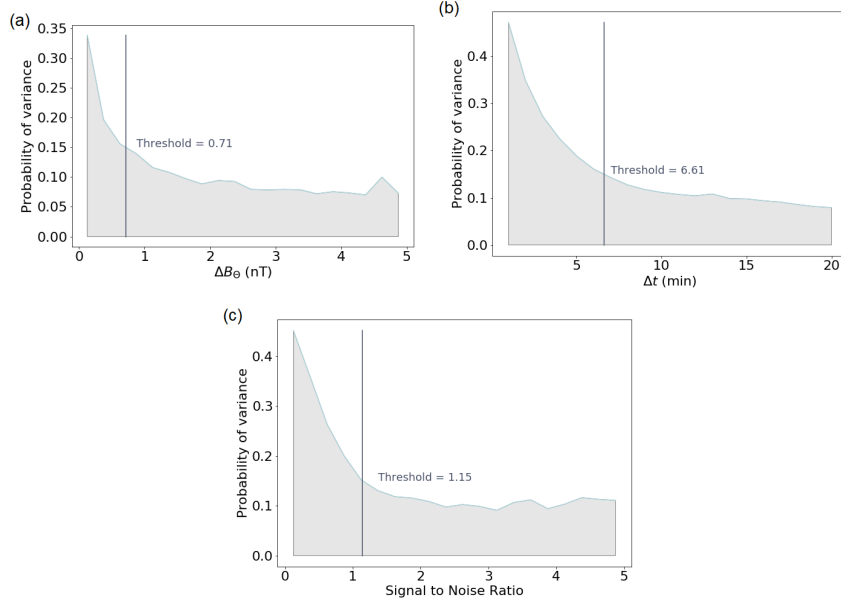


Figure 4. Comparisons of mean stability across the aforementioned five reconnection catalogues. Stability is analyzed using metrics of ΔB_θ , Δt , and signal to noise ratio for events. Events with a variance below a threshold of 0.15 are considered to validated for statistical analysis. This creates lower limit thresholds for ΔB_θ , Δt , and signal to noise ratio for events of 0.71 nT, 6.61 min, and 1.15 respectively.

S16 catalogue is one of stretched magnetic field lines reconnecting and releasing plasmoids downtail or dipolarizations planetward of the reconnection site. Reconnection in the day-side plasma sheet is likely to have a somewhat different morphology given the confinement by the magnetopause limiting the degree of current sheet stretch. Moreover, reconnection in the turbulent magnetosheath is also a process of likely different character to large-scale magnetotail reconfiguration.

3.1 Temporal Statistical Analysis

Figure 6 illustrates the temporal distribution of reconnection identified for the entirety of Cassini's lifetime for all events (dark blue), events within the magnetosphere (light blue), and the aforementioned thresholded events within the night-side magnetosphere (salmon). Notably, the three distributions are dissimilar due to the varying trajectory of Cassini's orbit throughout its lifetime, with the initial capture orbits following Saturn Orbit Insertion in 2004 favouring large radial distance detections (many in the solar wind and magnetosheath), in contrast to detections in 2017 during Cassini's proximal orbits favouring small radial distance identifications (inner to middle magnetosphere). Furthermore, no class of identifications maintains a consistent yearly rate of events due to these varying orbits. Most apparent are an absence of validated events present in 2008 due to Cassini entering a high-latitude polar orbit with small equatorial plane radial distances as indicated in Figure 2. The largest number of validated detections occur in 2006 and 2010 where Cassini entered into deep-tail equatorial orbits where it would be closest to the magnetotail current sheet, the site of reconnection. Hence, these years are likely the most accurate representation of magnetotail reconnection rates with ~ 900 yearly identifications. However, even during these orbits, Cassini is located out of these

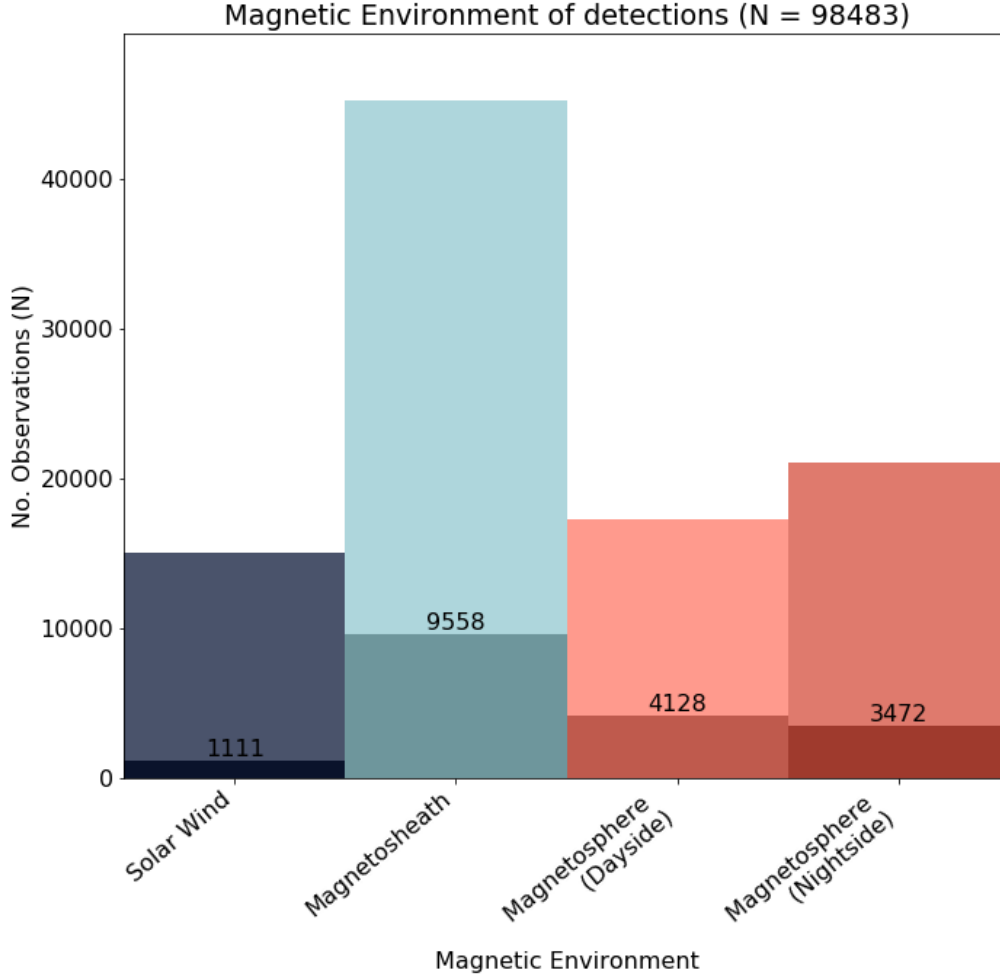


Figure 5. Number of identified events by Cassini during its near Saturn lifetime in the four magnetic environments: solar wind, in the planetary magnetosheath, day-side, and night-side magnetosphere. Reconnection events were classified into these regions by the Jackman et al. (2019) catalogue. Shaded regions of each classification represent the number of events that meet the thresholding criteria established in Figure 4.

spatial ranges for significant periods of time. Hence, the true number of identification for a spacecraft in an ideal location (N_{total}) can be calculated as:

$$N_{total} = N_i \frac{T_{total}}{T_i} \quad (2)$$

where N_i is number of validated events within limits (3472), T_{total} is the total time of Cassini's near Saturn lifetime (6.77×10^6 mins), and T_i is the total time where Cassini is within the magnetotail within $\pm 40^\circ$ latitude of the equatorial plane (2.48×10^6 mins). These values render an estimation of $N_{total} \approx 8895$ for Cassini's near Saturn lifetime, or 1.9 identifications per day.

The structures associated with magnetic reconnection are expected to initiate within the current sheet, where anti-parallel field lines meet (Harris, 1962; Connerney et al., 1983;

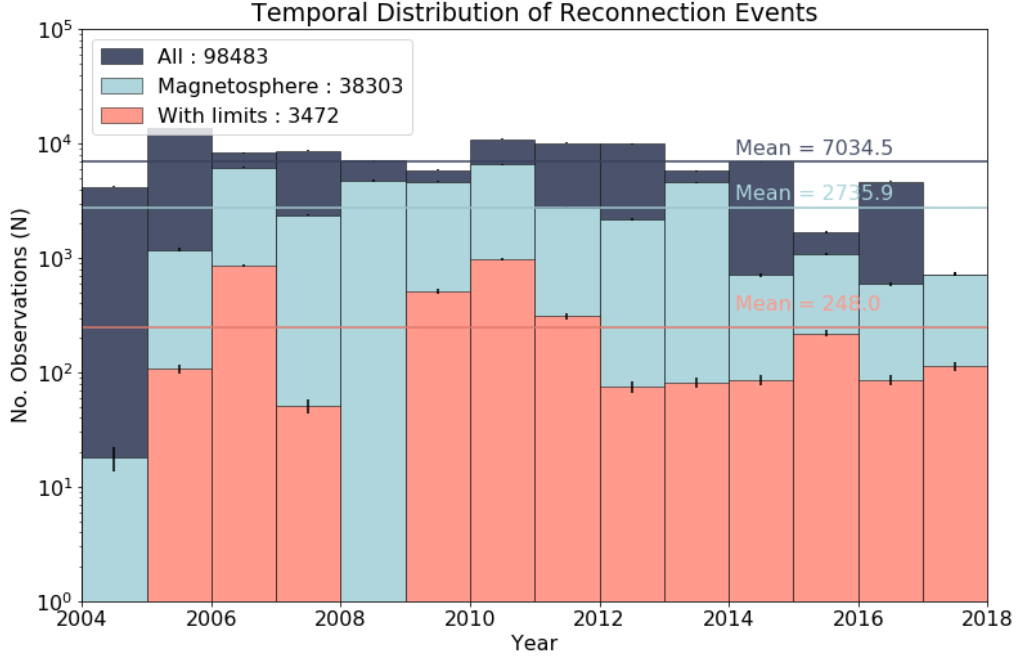


Figure 6. Yearly distribution of identified reconnection events during Cassini’s near Saturn lifetime for all (dark blue), magnetosphere (light blue, and night-side magnetosphere events within limitations established in Figure 4. On average, ~ 7000 events are identified yearly by the in-situ spacecraft, however, this does not account for all magnetospheric reconnections as only events that occur upwind of Cassini will be identifiable. Furthermore, this distribution does not account for the varying orbital trajectories of Cassini during its lifetime.

Arridge et al., 2008b). However, since Saturn’s axis has a seasonal tilt as it orbits the Sun and due to its large and expansive magnetosphere, its current sheet is known to become hinged with the seasonal variation of the planet (Arridge et al., 2008a; Carbary et al., 2015). This effect is visible in Figure 7 (a) and (b) which compares the latitude and radius of the aforementioned 3472 events in Kronian Radial-Theta-Phi (KRTP) coordinates across Cassini’s lifetime. KRTP coordinates are defined as the polar representation of a Cartesian coordinate system, where the x axis is positive Sun-ward in the Sun-Saturn line, the z axis is positive in the direction of Saturn’s north magnetic pole, and the y axis completes the right handed set. In 2004 Saturn experienced southern hemisphere summer, where the current sheet extends perpendicular to the rotational axis of the planet until $\sim 25 R_S$. Beyond this distance, the pressure of the incoming solar wind overcomes the planet’s magnetic pressure, causing the magnetotail to be swept out of the plane, creating a hinged magnetotail current sheet (Arridge et al., 2008a, 2011). Notably, an overall preference exists for negative latitude detections in 2004, whereas in 2017 a preference exists for positive latitude detections. This effect is due to the aforementioned current sheet hinging, which varies on the seasonal timescale of Saturn. This phenomenon is visible in the data where the large radial distance identifications occur close to 0° latitude, while identifications closer to the planet ($< 30 R_S$) follow the seasonal tilt variation of Saturn. In 2009, Saturn was experiencing an equinox. This means the current sheet is expected to have no hinging at this time, which is reflected by the reduced range of latitudinal detections during this period to being highly localized around 0° . However, the magnetotail current sheet does exhibit vertical flapping of the current sheet, closely linked to the Planetary Period Oscillations (PPOs) [e.g. Bradley et al. (2018)].

This flapping means that the current sheet can reach a modest range of latitude above/below its nominal central position. During 2009 and 2010, Cassini's trajectory was changed to an equatorial orbit with apokrone in the magnetotail at radial distances out to $\sim 50 R_S$, greatly facilitating the identification of magnetotail reconnection events. Other patterns of detections exist in this dataset, namely the extremely high and low latitude detections of 2007, mid 2009, 2013, and 2014. Identifications at these latitudes are due to the highly angled orbital trajectory of Cassini at these times (see Figure 2), where it comes close to the magnetopause boundary and hence may identify Kelvin-Helmholtz instabilities in magnetic field observations (Delamere et al., 2013b; Johnson et al., 2014; Burkholder et al., 2020). To reduce the impact of these detections, identifications within one hour of Cassini crossing the magnetopause were removed from the magnetosphere detections. When comparing these events with their number density it is apparent that these peculiar events are few in number and hence possibly a simple statistical error. The high latitude bins of 2013/2014 however exhibit > 10 detections in number density and hence can be considered statistically significant, they are at larger radial distances ($> 50 R_S$). This may imply these identifications are due to interactions with the magnetopause boundary or its nearby magnetic environment that are not removed by the Jackman et al. (2019) catalogue. This may be due to the spacecraft not crossing the boundary layer (Masters et al., 2011), but still orbiting close enough to be affected by its near plasma environment.

3.2 Spatial Statistical Analysis

Figure 8 indicates the spatial distribution of reconnection for all events in the G21 catalogue (dark blue), magnetosphere only (light blue), and night-side magnetosphere within the aforementioned limits (salmon). The distribution of events is described as functions of radial range (a), local time (b), and latitude (c). The majority of reconnection across all classes occurs in the 20-40 R_S range, however this is most likely due to Cassini spending much of its lifetime in this radial distance range, showing favour for detection at these distances. The local time distribution of reconnection is highly imbalanced in favour of dusk-side reconnection. This effect is most notable in the magnetospheric class where the number of dawn-side detections can be a factor of two times lower than dusk-side. However this effect still persists in our limited 3472 night-side events, with a high density of observations in the 18-21 hours range where the rotating magnetosphere enters a large scale expansion down tail. The latitudinal distribution of events is highly focused in the equatorial plane, particularly for the limited dataset. Identifications outside of the 20° -wide bin centred on 0° may be attributed to the observation of plasmoids near a current sheet which has two key physical phenomena controlling its location: (i) the seasonal variation and associated hinging of the current sheet, (ii) the vertical flapping accompanied by quasi-periodic thickening and thinning of the current sheet modulated by the planetary period, e.g. Provan et al. (2018) and references therein. Furthermore, a subset of the nightside detections correspond to TCRs as opposed to plasmoids, with the former being observable from the higher latitude lobes as opposed to the central current sheet region. Moreover, there is an expected lack of events at highest latitudes ($> \pm 70^\circ$) furthest from the theoretical sites where oppositely directed field lines from opposite hemispheres could merge and reconnect.

Figure 9 demonstrates global distribution of reconnection events within thresholds from Figure 4, but across all local times from three viewpoints at ~ 1600 (a), ~ 2000 (b), and ~ 0200 (c) hours local time. Night-side events are highly restricted to equatorial latitudes with maximal extents at $\sim 40^\circ$, with concentration centered around 0° latitude. Two relative hotspots exist in these night-side detections corresponding with the number of events at 2000 and 0200 hours local time from Figure 8. Day-side detections are observed to have a far larger latitudinal spread than night-side detections. Furthermore, two hotspots exist on the day-side, similar to night-side, however these are located at high latitudes ($\pm 40^\circ$) and restricted in local time (1400-1600 hours). Since these

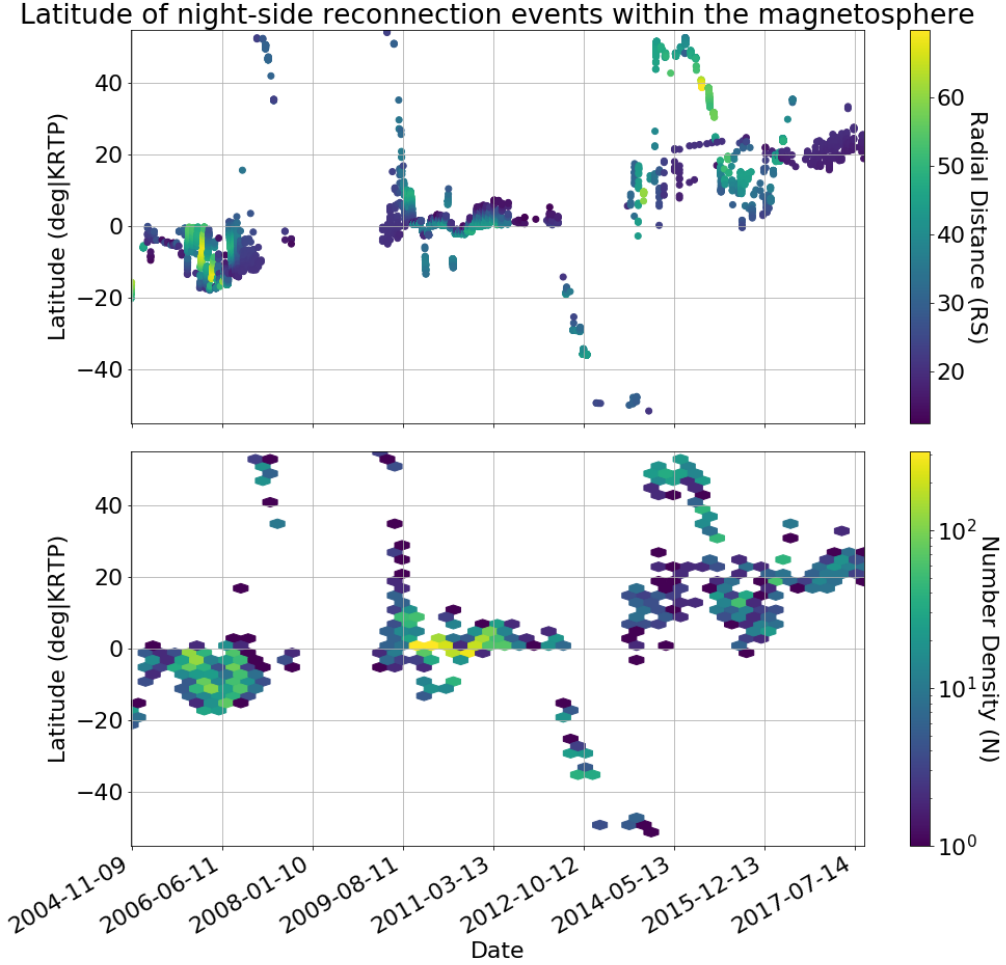


Figure 7. Reconnection occurrence as a function of latitude for the 3472 events in K RTP coordinates for the entirety of Cassini’s near-Saturn lifetime. Colour in these plots indicate (a) the radial distance of Cassini from Saturn during detection and (b) the number density of detections for given latitudes with time. The majority of reconnection is limited to the planetary current sheet, with variation from the 0 degrees latitude matching the expected long-term seasonal change of the planetary magnetic field.

identifications are on the day-side, where the machine learning algorithm has never been trained on, it is difficult to conclude these detections correspond to true events, however acknowledging them and their potential indication of some physical phenomenon other than reconnection makes them noteworthy observations.

Figure 10 demonstrates (a) an equatorial projection distribution of magnetospheric deflections (both day-side and night-side) and (b) the $|\Delta B_\theta|$ of events in these spatial bins. The occurrence distribution is normalized with respect to observation time of Cassini in each spatial bin, hence colour in this plot indicates the probability of identifying a reconnection event for every minute of observation in each spatial bin. Lack of colour in a given sector is attributed to either the Cassini spacecraft not exploring that region during its lifetime, or a lack of field deflection detections (despite Cassini sampling). Three main clusters of reconnection are identifiable in this figure, at 0300 - 0600, 1200 - 1700,

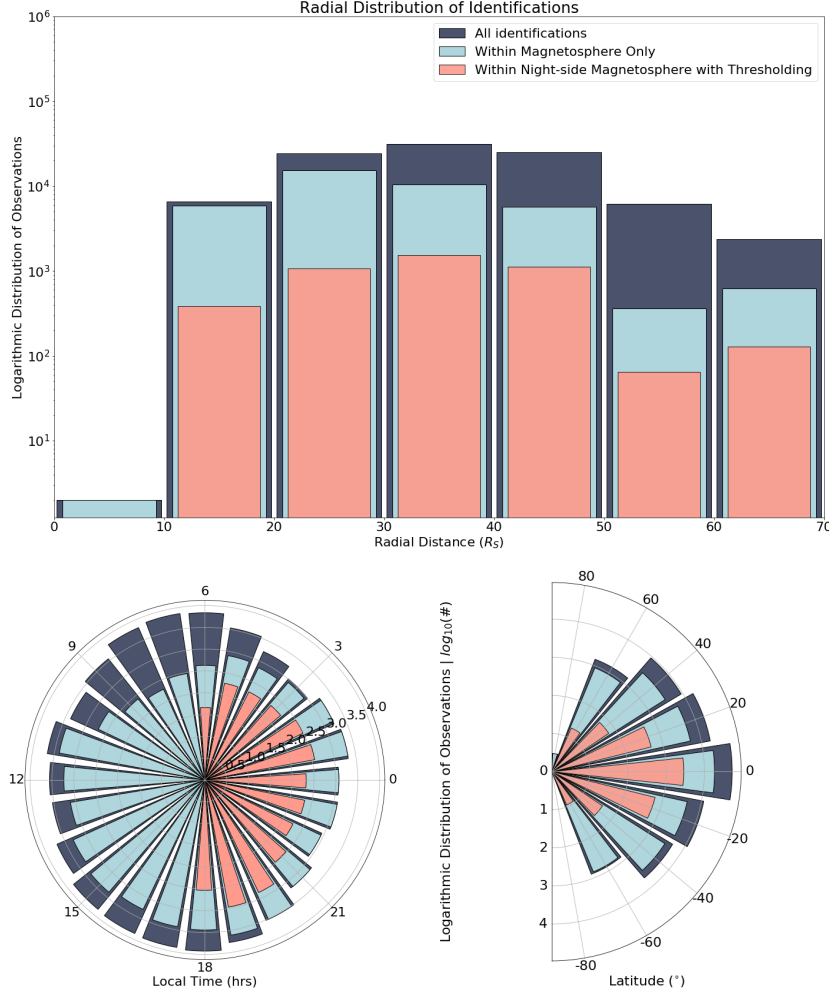


Figure 8. Radial (a), local time (b), and latitudinal (c) distributions of identified reconnection events for all events (dark blue), only events within the magnetosphere (light blue), and events within the magnetosphere and above the aforementioned parametric thresholds (salmon).

and 1900 - 0200 hours local time. The 0300 - 0600 local time cluster of reconnection probability is due a normalization effect. Very few detections (<10) exist in these spatial bins however the probability of identification is high due to Cassini occupying these bins for a small period of time, hence a high rate of error is associated with this cluster. Furthermore, these detections are close to the magnetopause boundary and are possibly due to near-boundary interactions. The cluster at 1200 - 1700 hours is associated with the two day-side hotspots of identifications discussed for Figure 9. Finally, the cluster of detections from 1900 - 0200 hours local time occur in statistically significant numbers and encompass a local time sector which was well sampled in the training data. This cluster represents the preferential region for identifying tail-side reconnection signatures. Unfortunately, the Cassini spacecraft has a lack of observations directly in the center of this cluster at ~ 2100 local time beyond $35 R_S$. This cluster may be far more populated with reconnection signatures if Cassini's trajectory had entered these spatial bins. Even with the lack of observations in these spatial bins it is still clear that a significant imbalance for detection exists in favour of dusk-side identifications. The $|\Delta B_\theta|$ plot shows a preference for larger deflection events to occur closer to the planet. This is likely due to magnetic field strength being stronger closer to the planet and typical signatures of deflec-

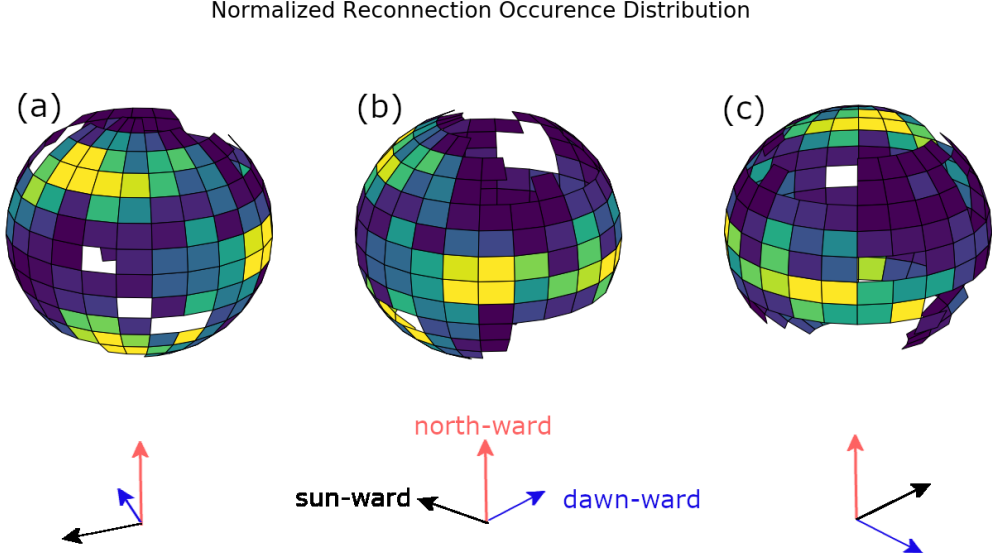


Figure 9. Normalized global distribution of identified reconnection events viewed from three different perspectives in a logarithmic colour scale from three viewpoints ~ 1600 (a), ~ 2000 (b), and ~ 0200 (c) hours local time.

tions featuring a polarity inversion. Hence, for a typical reconnection event, a larger ΔB_θ deflection would be expected closer to the planet. Also of note in this plot are the asymmetries between day and night-side, and dawn and dusk. Day-side show overall larger deflections than night-side for the same radial distances. This may be due to the unverified nature of these day-side identifications. It's possible that day-side reconnection facilitates the creation of stronger magnetic features. Alternatively it may be that due to this environment being so different to the night-side events the model was trained to identify, it can only consistently identify the larger magnetic deflection signatures. The dawn-dusk asymmetry is approximately inverse of the reconnection occurrence distribution. This may mean the apparent stronger magnetic signatures on the dawn side are a feature of uncertainty, or alternatively, it may imply that there is no asymmetry in flux transport for Saturn, merely that on the dusk-side, flux is transported often on small scale and that on the dawn-side flux is transported less frequently but in larger scales.

Figure 11 indicates the directionality of the 3472 validated magnetotail events normalized with respect to the mean number of observations in each $2.5 R_S$ bins. This normalization method better represents the directionality of events at a given radial distance for the imbalanced number of observations in both directions. The planetward (1162) and tailward (2310) classifications come directly from the G21 catalogue and can be inferred where positive to negative ΔB_θ events are considered to be planetward and tailward events exhibit a negative to positive ΔB_θ deflection. Notably, planetward event occur at lower radial distances on average ($32.8 R_S$) than tailward events ($34.7 R_S$), however a significant overlap exists between the two distributions making it difficult to distinctly classify them and hence identify the location of a planetary x-line.

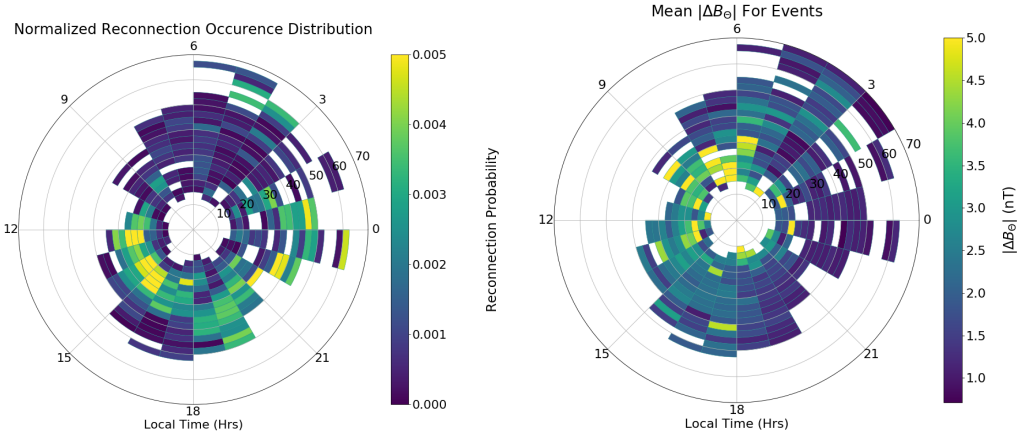


Figure 10. (a) Normalized radial distribution of identified reconnection events normalized for Cassini observing times in each spatial bin. (b) Mean $|\Delta B_\theta|$ for identified events in each radial and local time bins.

3.3 Parametric Statistical Analysis

The G21 catalogue extracts parametric information for each identified event. Figure 12 demonstrates the distribution of duration for the aforementioned 3472 events in log-log space, normalized to give the expected number of detection in each Δt bin in a single year. This method enables a first approximation of the size and frequency of events expected to be observed by an in-situ spacecraft, however, the scale of this distribution is highly dependant on the spacecraft trajectory and whether its orbit is favourable for tail-side reconnection detection. This distribution exhibits a power law relationship ($N = 299.23 \times \Delta t^{-1.28}$), which favours the theory of a scale invariant or fractal-like nature of the planetary magnetotail (Hoshino et al., 1994; Milovanov et al., 1996; Bradley et al., 2018). From this fit, it can be estimated that a spacecraft is expected to observe ~ 307 one minute duration events every year, however since these events (1) occur on such a short time scale, and (2) are likely to be very small compared to background magnetic topology, it is likely that these events will not be identified within magnetic field observations, however they provide a rough estimate of number and size of events for approximating mass loss for Saturn's magnetosphere. Similarly, extremely large and rare events can be approximated, for example a one in ten year event would have a yearly observation rate of $N = 1/10$, and from our power law fit, a duration of ~ 459 minutes. It is important to note that while this fit provides a potentially infinite size scale for reconnection events, in reality these events are limited in duration due to the finite scale of the magnetosphere and limitations on factors like flux tube content, inflow to the diffusion region (Goertz, 1983; Arridge et al., 2015). Some upper limit of duration exists, however during the 13 years of Cassini's observations, not enough reconnection events were detected to statistically conclude this upper limit.

Figure 13 demonstrates a similar parametric distribution of ΔB_θ for the 3472 events in log-log space, normalized to a year timescale. This distribution is also well described by a power law relationship ($N = 52.07 \times \Delta B_\theta^{-2.08}$). This distribution enables a similar level of predictability to reconnection event scale. The power law fit supports the idea for a fractal structure/scale invariant mechanism behind the creation of reconnection signatures. Furthermore, with this distribution it is possible to estimate yearly event occurrence for given ΔB_θ bins. Hence, it is expected to observe ~ 50 events with $0.875 < \Delta B_\theta < 1.125$, and it is expected to observe a single ~ 16 nT deflection event every ten years. It must be remembered that this distribution is also subject to the spatial lim-

Normalized Directionality of Magnetotail Events Within Limits (LT: 18 - 6)

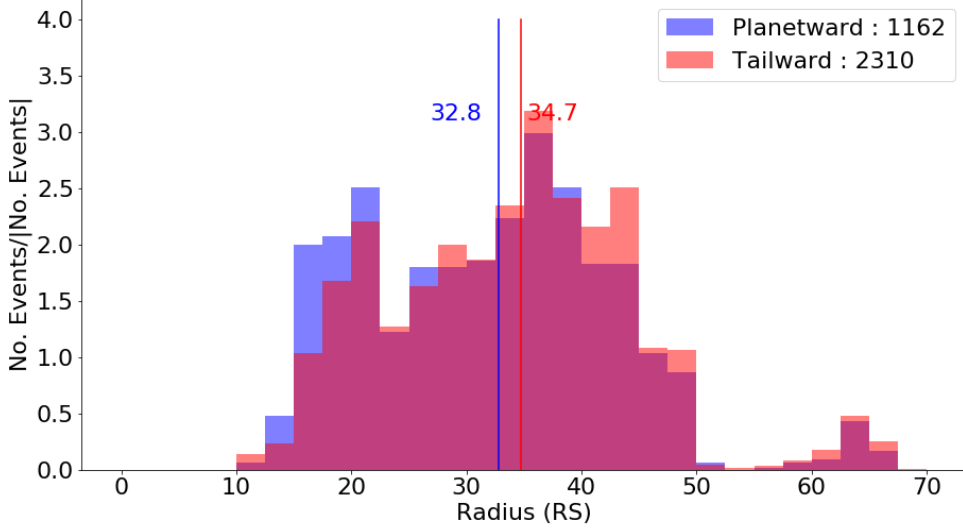


Figure 11. Radial distribution of planetward (blue) and tailward (red) events for night side identifications. Notably, planetward identifications are observed on average closer to the planet than tailward events, however there is a significant overlap of the two distributions.

itations of the Kronian magnetosphere and some upper limit of ΔB_θ exists that cannot be statistically identified exclusively using Cassini’s observations. For example, plasmoids can only be as wide as the total magnetotail width ($\sim 90 R_S$). In actuality, it is likely typical plasmoid sizes don’t approach these widths. This is inferred from research on relative sizes of plasmoids in Earth’s magnetosphere (Ieda et al., 1998). Plasmoids are created within the current sheet which itself has constraints on vertical extent [range 1-6 R_S , Giampieri and Dougherty (2004); Dougherty et al. (2005); Arridge et al. (2008b); Staniland et al. (2020)]. In practice, plasmoids represent localized bulges in the plasma sheet (as evidenced with the observation of TCRs) but there is a limit on this deformation of the current sheet. This creates strict spatial limitations on plasmoids. Similarly, ΔB_θ is limited by the available magnetic flux of Saturn, which is typically observed through variation in the auroral oval (Badman et al., 2005; Carbary, 2012; Badman et al., 2014). For this research, we assume that the spacecraft travels directly through the center of the identified plasmoid in a head-on trajectory, hence causing the maximum possible ΔB_θ deflection. In reality, it is likely the spacecraft intersects the majority of plasmoids in a glancing blow or off center trajectory causing a smaller observed ΔB_θ .

4 Discussion

As evidenced in the previous section, the ML catalogue created by G21 opens the path for statistical studies on the properties of magnetospheric reconnection for Saturn. This research has focused on a small, spatially restricted, validated dataset, and exclusively on the magnetic field properties as measured by Cassini.

From the temporal statistical analysis, we can conclude that spacecraft orbiting Saturn may sample ~ 200 magnetotail reconnection events every year. Spacecraft in deep-tail orbits are more likely to experience higher reconnection rates of ~ 900 events. However, through normalizing the total number of validated detections across Cassini’s lifetime (3472) with respect to time Cassini spent in the optimal spatial window for observ-

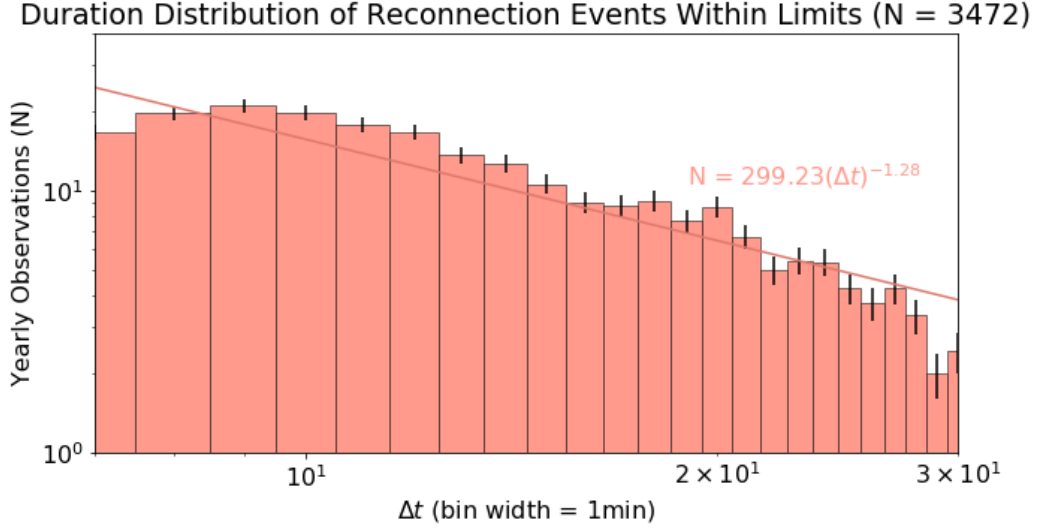


Figure 12. Log-log distribution of identified event duration for events longer than the aforementioned stability thresholds. This distribution is assumed to be exponential, with the implication being reconnection events are scale invariant, and is described by the equation: $N = 299.23 \times \Delta t^{-1.28}$.

ing magnetotail reconnection, an estimate of ~ 660 events occur yearly. This knowledge is crucial for establishing expectations for future spacecraft missions to Saturn. Furthermore, it can be concluded the seasonal variation and hinging of the current sheet for Saturn can be identified by analysing the locations of reconnection identification for tail-side events. While this dataset only covers ~ 14 years (less than half of the orbital period of Saturn), the latitudinal variation of detections follows closely the seasonal tilt of Saturn's magnetosphere. For the near current sheet latitudinal identifications, large radial distance observations occur more closely to 0° , while closer detections follow the planet's seasonal tilt. The shift between these two regimes occurs in the range of $20\text{--}30 R_S$ indicating a hinge in the planetary current sheet at $\sim 25 R_S$ which agrees with the theoretical location of the current sheet hinge for Saturn (Arridge et al., 2008a; Carbary et al., 2015). Notably, these findings are inclusive of plasmoids, TCRs, and dipolarizations. While plasmoids and TCR events are well constrained to the current sheet, dipolarizations are not and hence may have a wider latitudinal spread, hence causing near Saturn events ($<30 R_S$) to be observed at higher latitudes.

From the spatial distribution of events, it can be concluded that night-side magnetospheric reconnection signatures are most identified in the $20\text{--}40 R_S$ range, with a preference for the identification of many small-scale events in the dusk-side of the magnetosphere. This may imply a preference for Vasyliunas style reconnection over Dungey cycle style (Badman & Cowley, 2007). Vasyliunas reconnection is associated with mass loss and Dungey cycle reconnection is associated with both mass loss and flux closure. Hence, this preference for Vasyliunas style reconnection favours a loss of mass with no change in the ratio of open and closed magnetic fields. Furthermore, observations of reconnection are localized to the equatorial plane, particularly for night-side reconnection. This can be explained as reconnection occurs localized within the planetary current sheet and signatures of reconnection travelling along the current sheet. Also of note, dayside field deflections from the catalogue, while not validated, seem to be observed across a broader range of latitude and longitude with notable hotspots at $\pm 40^\circ$. It is hard to say

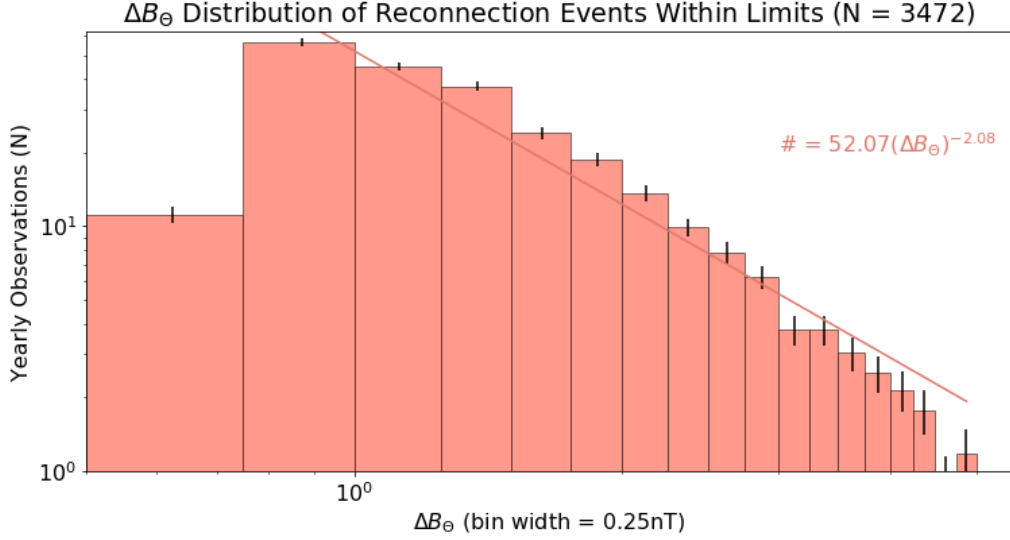


Figure 13. Log-log distribution of identified event north-south magnetic deflection for events above the aforementioned stability thresholds. Assuming these events are scale invariant, an exponential line is fit to the distribution, of the order $N = 52.07 \times \Delta B_{\theta}^{-2.08}$.

what might cause these hotspots, however, if these detections are indicative of some underlying phenomenon, it would be an interesting avenue for future research on day-side magnetospheric reconnection.

From the research on directionality of reconnection events and the highly overlapped distribution of tailward and planetward events, it is concluded that either the planetary x-line is highly mobile across the 14 year period, or that its location is beyond Cassini's observing window for much of the time. Previous studies at the gas giants have sought to explore the x-line location and properties. Vogt et al. (2010) examined Galileo data at Jupiter and found a reasonably clear, statistically significant boundary between tailward and planetward events, indicating a jovian tail x-line at $\sim 90 R_J$ at dawn, and $\sim 120 R_J$ at dusk. More recently, Vogt et al. (2020) took a similar approach to event identification and performed a statistical analysis of Juno magnetometer data. That study did not reveal a statistical x-line position. Thomsen et al. (2014) studied plasma flow parameters at Saturn and found that no quasi-steady x-line position was found within $45 R_S$. From Figure 11 an unstable equilibrium point may exist at $\sim 33.75 R_S$ that the x-line will tend to on average, however it is likely that due to the variable nature of Saturn's magnetic field and the surrounding solar wind, the location of the x-line is equally as variable (Jia et al., 2012; Smith et al., 2016, 2018a). The coverage of the terrestrial magnetotail allows for examination of both the near-Earth and the distant tail x-line (Ieda et al., 1998; Eastwood et al., 2005; Imber et al., 2011). Jackman and Arridge (2011b) noted that the down-tail coverage at Jupiter and Saturn equates to $\sim <3$ times the typical magnetopause standoff distance at those planets, whereas the coverage at Earth with spacecraft like Geotail $\sim 200 R_E$ equates to ~ 20 times the typical terrestrial standoff distance. Thus the exploration space at the gas giants is much more limited. By applying simple scaling from Earth to account for the planetary magnetic field strength, the magnetopause standoff distance, and the observed terrestrial near-planet x-line location, one might expect Saturn's x-line to lie $\sim 75 R_S$ from the planet on average (Jackman et al., 2014). However, it must be noted that Earth's magnetosphere is Dungey cycle dominated and hence its phenomenon may not be directly transferable in this manner. Since Cassini spent

the majority of observations planetwards of this distance, this theoretical location cannot be confirmed with this research.

From the parametric distribution of events, it is concluded that Saturn's magnetotail has a fractal-like nature for reconnection, i.e. the same underlying processes create both large and small events with an inverse power law distribution of occurrence. This type of distribution is similar to scale size found for magnetohydrodynamic modelling of magnetic islands (Fermo et al., 2010), and in the size distributions of reconnection products in other magnetospheres (Fermo et al., 2011; Akhavan-Tafti et al., 2018; Smith et al., 2018c). This relationship is true for both the duration (Δt) and the deflection in northward magnetic field (ΔB_θ). In Section 3.1, the reconnection rate for Saturn's magnetotail was found to be ~ 1.9 reconnection events per day, however this only accounts for events above our statistical thresholds ($\Delta t > 6.61$ mins). From the distribution of Δt , this reconnection rate can be corrected to include small events through the solving of the integrals:

$$1.9 = c \int_{6.61}^{\infty} 299.23 \Delta t^{-1.28} d\Delta t \quad (3)$$

$$RR_{corr} = c \int_1^{\infty} 299.23 \Delta t^{-1.28} d\Delta t \quad (4)$$

where RR_{corr} is the true reconnection rate for plasmoids and is calculated to be 3.22 reconnection events per day.

Similarly, from the Δt distribution and previous studies of plasmoid properties, it is possible to estimate the mass loss in Saturn's magnetotail as:

$$M = \rho V \quad (5)$$

$$M = \rho W H v \Delta t \quad (6)$$

where ρ represents the density of the plasmoid (0.1 cm^{-3} of 16 amu ions; Thomsen et al. (2014)), V is the volume of the plasmoid (assumed to be a cuboid for simplicity), W is the width of the plasmoid (90 R_S upper limit at full tail width; Jackman et al. (2014)), H is the height of the plasmoid (4 R_S ; Kellett et al. (2009); Arridge et al. (2011); Sergis et al. (2011); Szego et al. (2012); Staniland et al. (2020)), and v is the velocity of the moving plasmoid (300 km s^{-1} ; Jackman et al. (2014)). Inserting these values and solving for M gives:

$$M = 524.31 \Delta t \quad (7)$$

where Δt is in seconds. By taking the duration distribution of identified events from Figure 12, with a maximum observed duration of 400 minutes (from the G21 catalogue) as the upper limit on length ($L = v \Delta t \approx 120 R_S$), the mean mass per plasmoid can be calculated as $9.22 \times 10^5 \text{ kg}$. Taking the aforementioned reconnection rate of 3.22, this gives an estimate upper limit of mass loss through plasmoids of 34.4 kg s^{-1} . This finding aligns with previous estimates of Kronian plasmoid mass and mass loss rates (Bagenal & Delamere, 2011; Jackman et al., 2014). Comparing this mass loss rate to the mass loading rate from Enceladus ($8\text{-}250 \text{ kg s}^{-1}$) suggests a sizeable role for a viscous like interaction at Saturn (Delamere & Bagenal, 2013a; Delamere et al., 2018).

The G21 catalogue opens a new avenue for planetary magnetospheric research by providing the most comprehensive catalogue of magnetic field deflections in the Saturn

system, covering 14 years of Cassini data, different Saturn seasons and an entire solar cycle. This paper provides an investigation of reconnection events identified within, with a heavy focus on night-side magnetospheric activity. However, this research can be built upon to investigate signatures of day-side reconnection, or for the events located in the magnetosheath or solar wind. Investigations into all identified events along with a comparison of plasma properties from the CAPS plasma spectrometer may render further understanding of reconnection, and bulk plasma flow within the magnetosphere. Finally, the ML method applied to the Cassini observations may be expanded, and retrained for missions that have focused on other planets in our solar system such as MESSENGER at Mercury, and Galileo or Juno at Jupiter.

Data Availability Statement

Calibrated data from the Cassini mission are available from the NASA Planetary Data System at the Jet Propulsion Laboratory [<https://pds.jpl.nasa.gov/>].

The datasets created from this study can be found on Zenodo [DOI: 10.5281/zenodo.4638961].

Acknowledgments

T.M.G.'s work is supported by the Science and Technology Facilities Council Opportunities Fund Grant ST/T002255/1 and by the Alan Turing Institute Grant EP/N510129/1.

C. M. J.'s work is supported by the Science Foundation Ireland Grant 18/FRL/6199.

A. W. S is supported by STFC Consolidated Grant ST/S000240/1 and NERC grant NE/P017150/1

References

- Akhavan-Tafti, M., Slavin, J. A., Le, G., Eastwood, J. P., Strangeway, R. J., Russell, C. T., ... Burch, J. L. (2018). MMS examination of FTEs at the Earth's subsolar magnetopause. *Journal of Geophysical Research: Space Physics*, 123(2), 1224-1241. Retrieved from <https://agupubs.onlinelibrary.wiley.com/doi/abs/10.1002/2017JA024681> doi: <https://doi.org/10.1002/2017JA024681>
- Arridge, C. S., André, N., Khurana, K. K., Russell, C. T., Cowley, S. W. H., Provan, G., ... Young, D. T. (2011). Periodic motion of Saturn's nightside plasma sheet. *Journal of Geophysical Research: Space Physics*, 116(A11). Retrieved from <https://agupubs.onlinelibrary.wiley.com/doi/abs/10.1029/2011JA016827> doi: <https://doi.org/10.1029/2011JA016827>
- Arridge, C. S., Eastwood, J. P., Jackman, C. M., Poh, G.-K., Slavin, J. A., Thomsen, M. F., ... et al. (2015). Cassini in situ observations of long-duration magnetic reconnection in Saturn's magnetotail. *Nature Physics*, 12(3), 268-271. Retrieved from <http://dx.doi.org/10.1038/nphys3565> doi: <https://doi.org/10.1038/nphys3565>
- Arridge, C. S., Khurana, K. K., Russell, C. T., Southwood, D. J., Achilleos, N., Dougherty, M. K., ... Leinweber, H. K. (2008a). Warping of Saturn's magnetospheric and magnetotail current sheets. *Journal of Geophysical Research: Space Physics*, 113(A8). Retrieved from <https://agupubs.onlinelibrary.wiley.com/doi/abs/10.1029/2007JA012963> doi: <https://doi.org/10.1029/2007JA012963>
- Arridge, C. S., Russell, C. T., Khurana, K. K., Achilleos, N., Cowley, S. W. H., Dougherty, M. K., ... Bunce, E. J. (2008b). Saturn's magnetodisc current sheet. *Journal of Geophysical Research: Space Physics*, 113(A4). Retrieved from <https://agupubs.onlinelibrary.wiley.com/doi/abs/10.1029/2007JA012540> doi: <https://doi.org/10.1029/2007JA012540>

- Azari, A. R., Biersteker, J. B., Dewey, R. M., Doran, G., Forsberg, E. J., Harris, C. D. K., ... Ruhunusiri, S. (2020). Integrating machine learning for planetary science: Perspectives for the next decade. *White Paper Submitted to the Decadal Survey on Planetary Science and Astrobiology 2023-2032*. Retrieved from <https://arxiv.org/abs/2007.15129>
- Bader, A., Badman, S. V., Yao, Z. H., Kinrade, J., & Pryor, W. R. (2019). Observations of continuous quasiperiodic auroral pulsations on Saturn in high time-resolution UV auroral imagery. *Journal of Geophysical Research: Space Physics*, 124(4), 2451-2465. Retrieved from <https://agupubs.onlinelibrary.wiley.com/doi/abs/10.1029/2018JA026320> doi: <https://doi.org/10.1029/2018JA026320>
- Badman, S. V., Bonfond, B., Fujimoto, M., Gray, R. L., Kasaba, Y., Kasahara, S., ... Yoshioka, K. (2016). Weakening of Jupiter's main auroral emission during January 2014. *Geophysical Research Letters*, 43(3), 988-997. Retrieved from <https://agupubs.onlinelibrary.wiley.com/doi/abs/10.1002/2015GL067366> doi: <https://doi.org/10.1002/2015GL067366>
- Badman, S. V., Bunce, E. J., Clarke, J. T., Cowley, S. W. H., Gérard, J.-C., Grodent, D., & Milan, S. E. (2005). Open flux estimates in Saturn's magnetosphere during the January 2004 Cassini-HST campaign, and implications for reconnection rates. *Journal of Geophysical Research: Space Physics*, 110(A11). Retrieved from <https://agupubs.onlinelibrary.wiley.com/doi/abs/10.1029/2005JA011240> doi: <https://doi.org/10.1029/2005JA011240>
- Badman, S. V., & Cowley, S. W. H. (2007). Significance of Dungey-cycle flows in Jupiter's and Saturn's magnetospheres, and their identification on closed equatorial field lines. *Annales Geophysicae*, 25(4), 941-951. doi: [10.5194/angeo-25-941-2007](https://doi.org/10.5194/angeo-25-941-2007)
- Badman, S. V., Jackman, C. M., Nichols, J. D., Clarke, J. T., & Gérard, J.-C. (2014). Open flux in Saturn's magnetosphere. *Icarus*, 231, 137-145. Retrieved from <https://www.sciencedirect.com/science/article/pii/S0019103513005137> doi: <https://doi.org/10.1016/j.icarus.2013.12.004>
- Badman, S. V., Masters, A., Hasegawa, H., Fujimoto, M., Radioti, A., Grodent, D., ... Coates, A. (2013). Bursty magnetic reconnection at Saturn's magnetopause. *Geophysical Research Letters*, 40(6), 1027-1031. Retrieved from <https://agupubs.onlinelibrary.wiley.com/doi/abs/10.1002/grl.50199> doi: <https://doi.org/10.1002/grl.50199>
- Bagenal, F., & Delamere, P. A. (2011). Flow of mass and energy in the magnetospheres of Jupiter and Saturn. *Journal of Geophysical Research: Space Physics*, 116(A5). Retrieved from <https://agupubs.onlinelibrary.wiley.com/doi/abs/10.1029/2010JA016294> doi: <https://doi.org/10.1029/2010JA016294>
- Bradley, T. J., Cowley, S. W. H., Bunce, E. J., Smith, A. W., Jackman, C. M., & Provan, G. (2018). Planetary period modulation of reconnection bursts in Saturn's magnetotail. *Journal of Geophysical Research: Space Physics*, 123(11), 9476-9507. Retrieved from <https://agupubs.onlinelibrary.wiley.com/doi/abs/10.1029/2018JA025932> doi: <https://doi.org/10.1029/2018JA025932>
- Bunce, E. J., Cowley, S. W. H., Wright, D. M., Coates, A. J., Dougherty, M. K., Krupp, N., ... Rymer, A. M. (2005). In situ observations of a solar wind compression-induced hot plasma injection in Saturn's tail. *Geophysical Research Letters*, 32(20). Retrieved from <https://agupubs.onlinelibrary.wiley.com/doi/abs/10.1029/2005GL022888> doi: [10.1029/2005GL022888](https://doi.org/10.1029/2005GL022888)
- Burkholder, B. L., Delamere, P. A., Johnson, J. R., & Ng, C.-S. (2020). Identifying active Kelvin-Helmholtz vortices on Saturn's magnetopause boundary. *Geophysical Research Letters*, 47(1), e2019GL084206. Retrieved from <https://agupubs.onlinelibrary.wiley.com/doi/abs/10.1029/2019GL084206>

- (e2019GL084206 10.1029/2019GL084206) doi: <https://doi.org/10.1029/2019GL084206>
- Carbary, J. F. (2012). The morphology of Saturn's ultraviolet aurora. *Journal of Geophysical Research: Space Physics*, 117(A6). Retrieved from <https://agupubs.onlinelibrary.wiley.com/doi/abs/10.1029/2012JA017670> doi: <https://doi.org/10.1029/2012JA017670>
- Carbary, J. F., Sergis, N., Mitchell, D. G., & Krupp, N. (2015). Saturn's hinge parameter from Cassini magnetotail passes in 2013–2014. *Journal of Geophysical Research: Space Physics*, 120(6), 4438–4445. Retrieved from <https://agupubs.onlinelibrary.wiley.com/doi/abs/10.1002/2015JA021152> doi: <https://doi.org/10.1002/2015JA021152>
- Chen, Y., Hill, T. W., Rymer, A. M., & Wilson, R. J. (2010). Rate of radial transport of plasma in Saturn's inner magnetosphere. *Journal of Geophysical Research: Space Physics*, 115(A10). Retrieved from <https://agupubs.onlinelibrary.wiley.com/doi/abs/10.1029/2010JA015412> doi: <https://doi.org/10.1029/2010JA015412>
- Connerney, J. E. P., Acuña, M. H., & Ness, N. F. (1983). Currents in Saturn's magnetosphere. *Journal of Geophysical Research: Space Physics*, 88(A11), 8779–8789. Retrieved from <https://agupubs.onlinelibrary.wiley.com/doi/abs/10.1029/JA088iA11p08779> doi: <https://doi.org/10.1029/JA088iA11p08779>
- Delamere, P. A., & Bagenal, F. (2013a). Magnetotail structure of the giant magnetospheres: Implications of the viscous interaction with the solar wind. *Journal of Geophysical Research: Space Physics*, 118(11), 7045–7053. Retrieved from <https://agupubs.onlinelibrary.wiley.com/doi/abs/10.1002/2013JA019179> doi: <https://doi.org/10.1002/2013JA019179>
- Delamere, P. A., Burkholder, B., & Ma, X. (2018). Three-dimensional hybrid simulation of viscous-like processes at Saturn's magnetopause boundary. *Geophysical Research Letters*, 45(16), 7901–7908. Retrieved from <https://agupubs.onlinelibrary.wiley.com/doi/abs/10.1029/2018GL078922> doi: <https://doi.org/10.1029/2018GL078922>
- Delamere, P. A., Otto, A., Ma, X., Bagenal, F., & Wilson, R. J. (2015). Magnetic flux circulation in the rotationally driven giant magnetospheres. *Journal of Geophysical Research: Space Physics*, 120(6), 4229–4245. Retrieved from <https://agupubs.onlinelibrary.wiley.com/doi/abs/10.1002/2015JA021036> doi: <https://doi.org/10.1002/2015JA021036>
- Delamere, P. A., Wilson, R. J., Eriksson, S., & Bagenal, F. (2013b). Magnetic signatures of Kelvin-Helmholtz vortices on Saturn's magnetopause: Global survey. *Journal of Geophysical Research: Space Physics*, 118(1), 393–404. Retrieved from <https://agupubs.onlinelibrary.wiley.com/doi/abs/10.1029/2012JA018197> doi: <https://doi.org/10.1029/2012JA018197>
- Dougherty, M. K., Achilleos, N., Andre, N., Arridge, C. S., Balogh, A., Bertucci, C., ... Tsurutani, B. T. (2005). Cassini magnetometer observations during Saturn orbit insertion. *Science*, 307(5713), 1266–1270. Retrieved from <https://science.sciencemag.org/content/307/5713/1266> doi: [10.1126/science.1106098](https://doi.org/10.1126/science.1106098)
- Dungey, J. W. (1961). Interplanetary magnetic field and the auroral zones. *Phys. Rev. Lett.*, 6, 47–48. Retrieved from <https://link.aps.org/doi/10.1103/PhysRevLett.6.47> doi: [10.1103/PhysRevLett.6.47](https://doi.org/10.1103/PhysRevLett.6.47)
- Dungey, J. W. (1965). The Length of the Magnetospheric Tail. *Journal of Geophysical Research*, 70(7), 1753–1753. doi: [10.1029/JZ070i007p01753](https://doi.org/10.1029/JZ070i007p01753)
- Eastwood, J. P., Sibeck, D. G., Slavin, J. A., Goldstein, M. L., Lavraud, B., Sitnov, M., ... Dandouras, I. (2005). Observations of multiple x-line structure in the Earth's magnetotail current sheet: A Cluster case study. *Geophysical Research Letters*, 32(11). Retrieved from <https://agupubs.onlinelibrary.wiley.com/doi/abs/10.1029/2005GL022509> doi: <https://doi.org/10.1029/2005GL022509>

- <https://doi.org/10.1029/2005GL022509>
- Fermo, R. L., Drake, J. F., & Swisdak, M. (2010). A statistical model of magnetic islands in a current layer. *Physics of Plasmas*, 17(1), 010702. Retrieved from <https://doi.org/10.1063/1.3286437> doi: 10.1063/1.3286437
- Fermo, R. L., Drake, J. F., Swisdak, M., & Hwang, K.-J. (2011). Comparison of a statistical model for magnetic islands in large current layers with Hall MHD simulations and Cluster FTE observations. *Journal of Geophysical Research: Space Physics*, 116(A9). Retrieved from <https://agupubs.onlinelibrary.wiley.com/doi/abs/10.1029/2010JA016271> doi: <https://doi.org/10.1029/2010JA016271>
- Fleshman, B. L., Delamere, P. A., & Bagenal, F. (2010). The Source of Saturn's Extended Neutral Cloud. In *Agu fall meeting abstracts* (Vol. 2010, p. SM11C-1768).
- Garton, T. M. (2020). *GartontT/SaturnML: Updated catalogue (Version 1.0)*. Zenodo. Retrieved from <https://doi.org/10.5281/zenodo.4638961> doi: 10.5281/zenodo.4638961
- Garton, T. M., Jackman, C. M., Smith, A. W., Yeakel, K. L., Maloney, S. A., & Vande-griff, J. (2021). Machine learning applications to kronian magnetospheric reconnection classification. *Frontiers in Astronomy and Space Sciences*, 7, 104. Retrieved from <https://www.frontiersin.org/article/10.3389/fspas.2020.600031> doi: 10.3389/fspas.2020.600031
- Geirhos, R., Janssen, D. H. J., Schütt, H. H., Rauber, J., Bethge, M., & Wichmann, F. A. (2018). *Comparing deep neural networks against humans: object recognition when the signal gets weaker*.
- Giampieri, G., & Dougherty, M. K. (2004). Modelling of the ring current in Saturn's magnetosphere. *Annales Geophysicae*, 22(2), 653–659. Retrieved from <https://angeo.copernicus.org/articles/22/653/2004/> doi: 10.5194/angeo-22-653-2004
- Goertz, C. K. (1983). Detached plasma in Saturn's front side magnetosphere. *Geophysical Research Letters*, 10(6), 455–458. Retrieved from <https://agupubs.onlinelibrary.wiley.com/doi/abs/10.1029/GL010i006p00455> doi: <https://doi.org/10.1029/GL010i006p00455>
- Guo, R., Yao, Z., Wei, Y., Ray, L., Rae, I., Arridge, C., ... Dougherty, M. (2018). Rotationally driven magnetic reconnection in Saturn's dayside. *Nature Astronomy*, 2. doi: 10.1038/s41550-018-0461-9
- Harris, E. G. (1962). On a plasma sheath separating regions of oppositely directed magnetic field. *Il Nuovo Cimento (1955-1965)*, 23(1), 115–121.
- He, K., Zhang, X., Ren, S., & Sun, J. (2015). Delving deep into rectifiers: Surpassing human-level performance on ImageNet classification. In *Proceedings of the 2015 IEEE international conference on computer vision (iccv)* (p. 1026–1034). USA: IEEE Computer Society. Retrieved from <https://doi.org/10.1109/ICCV.2015.123> doi: 10.1109/ICCV.2015.123
- Hesse, M., & Cassak, P. A. (2020). Magnetic reconnection in the space sciences: Past, present, and future. *Journal of Geophysical Research: Space Physics*, 125(2), e2018JA025935. Retrieved from <https://agupubs.onlinelibrary.wiley.com/doi/abs/10.1029/2018JA025935> (e2018JA025935 2018JA025935) doi: <https://doi.org/10.1029/2018JA025935>
- Hill, T. W., Thomsen, M. F., Henderson, M. G., Tokar, R. L., Coates, A. J., McAndrews, H. J., ... Young, D. T. (2008). Plasmoids in Saturn's magnetotail. *Journal of Geophysical Research: Space Physics*, 113(A1). Retrieved from <https://agupubs.onlinelibrary.wiley.com/doi/abs/10.1029/2007JA012626> doi: 10.1029/2007JA012626
- Hones, J., E. W. (1977). Substorm processes in the magnetotail: Comments on 'On hot tenuous plasmas, fireballs, and boundary layers in the Earth's magnetotail' by L. A. Frank, K. L. Ackerson, and R. P. Lepping. *Journal of Geophysical*

- Research*, 82(35), 5633. doi: 10.1029/JA082i035p05633
- Hoshino, M., Nishida, A., Yamamoto, T., & Kokubun, S. (1994). Turbulent magnetic field in the distant magnetotail: Bottom-up process of plasmoid formation? *Geophysical Research Letters*, 21(25), 2935-2938. Retrieved from <https://agupubs.onlinelibrary.wiley.com/doi/abs/10.1029/94GL02094> doi: <https://doi.org/10.1029/94GL02094>
- Huang, S., Zhao, P., He, J., Yuan, Z., Zhou, M., Fu, H., ... Burch, J. (2018). A new method to identify flux ropes in space plasmas. *Annales Geophysicae*, 36(5), 1275-1283. Retrieved from <https://angeo.copernicus.org/articles/36/1275/2018/> doi: 10.5194/angeo-36-1275-2018
- Huddleston, D. E., Russell, C. T., Le, G., & Szabo, A. (1997). Magnetopause structure and the role of reconnection at the outer planets. *Journal of Geophysical Research: Space Physics*, 102(A11), 24289-24004. doi: 10.1029/97JA02416
- Ieda, A., Machida, S., Mukai, T., Saito, Y., Yamamoto, T., Nishida, A., ... Kokubun, S. (1998). Statistical analysis of the plasmoid evolution with Geotail observations. *Journal of Geophysical Research: Space Physics*, 103(A3), 4453-4465. Retrieved from <https://agupubs.onlinelibrary.wiley.com/doi/abs/10.1029/97JA03240> doi: <https://doi.org/10.1029/97JA03240>
- Imber, S. M., Slavin, J. A., Auster, H. U., & Angelopoulos, V. (2011). A THEMIS survey of flux ropes and traveling compression regions: Location of the near-Earth reconnection site during solar minimum. *Journal of Geophysical Research: Space Physics*, 116(A2). Retrieved from <https://agupubs.onlinelibrary.wiley.com/doi/abs/10.1029/2010JA016026> doi: <https://doi.org/10.1029/2010JA016026>
- Jabbar, H., & Khan, R. Z. (2015). Methods to avoid over-fitting and under-fitting in supervised machine learning (comparative study). *Computer Science, Communication and Instrumentation Devices*, 163-172.
- Jackman, C. M., Achilleos, N., Cowley, S. W., Bunce, E. J., Radioti, A., Grodent, D., ... Pryor, W. (2013). Auroral counterpart of magnetic field dipolarizations in Saturn's tail. *Planetary and Space Science*, 82-83, 34 - 42. Retrieved from <http://www.sciencedirect.com/science/article/pii/S003206331300069X> doi: <https://doi.org/10.1016/j.pss.2013.03.010>
- Jackman, C. M., & Arridge, C. S. (2011b). Statistical properties of the magnetic field in the Kronian magnetotail lobes and current sheet. *Journal of Geophysical Research: Space Physics*, 116(A5). Retrieved from <https://agupubs.onlinelibrary.wiley.com/doi/abs/10.1029/2010JA015973> doi: <https://doi.org/10.1029/2010JA015973>
- Jackman, C. M., Arridge, C. S., Krupp, N., Bunce, E. J., Mitchell, D. G., McAndrews, H. J., ... Coates, A. J. (2008). A multi-instrument view of tail reconnection at Saturn. *Journal of Geophysical Research (Space Physics)*, 113(A11), A11213. doi: 10.1029/2008JA013592
- Jackman, C. M., Lamy, L., Freeman, M. P., Zarka, P., Cecconi, B., Kurth, W. S., ... Dougherty, M. K. (2009). On the character and distribution of lower-frequency radio emissions at Saturn and their relationship to substorm-like events. *Journal of Geophysical Research: Space Physics*, 114(A8). Retrieved from <https://agupubs.onlinelibrary.wiley.com/doi/abs/10.1029/2008JA013997> doi: <https://doi.org/10.1029/2008JA013997>
- Jackman, C. M., Russell, C. T., Southwood, D. J., Arridge, C. S., Achilleos, N., & Dougherty, M. K. (2007). Strong rapid dipolarizations in Saturn's magnetotail: In situ evidence of reconnection. *Geophysical Research Letters*, 34(11). Retrieved from <https://agupubs.onlinelibrary.wiley.com/doi/abs/10.1029/2007GL029764> doi: 10.1029/2007GL029764
- Jackman, C. M., Slavin, J. A., & Cowley, S. W. H. (2011a). Cassini observations of plasmoid structure and dynamics: Implications for the role of magnetic reconnection in magnetospheric circulation at Saturn. *Journal of*

- 817 *Geophysical Research: Space Physics*, 116(A10). Retrieved from [https://](https://agupubs.onlinelibrary.wiley.com/doi/abs/10.1029/2011JA016682)
 818 agupubs.onlinelibrary.wiley.com/doi/abs/10.1029/2011JA016682 doi:
 819 <https://doi.org/10.1029/2011JA016682>
- 820 Jackman, C. M., Slavin, J. A., Kivelson, M. G., Southwood, D. J., Achilleos, N.,
 821 Thomsen, M. F., ... Vogt, M. F. (2014). Saturn's dynamic magnetotail: A
 822 comprehensive magnetic field and plasma survey of plasmoids and traveling
 823 compression regions and their role in global magnetospheric dynamics. *Jour-*
 824 *nal of Geophysical Research: Space Physics*, 119(7), 5465-5494. Retrieved
 825 from [https://agupubs.onlinelibrary.wiley.com/doi/abs/10.1002/](https://agupubs.onlinelibrary.wiley.com/doi/abs/10.1002/2013JA019388)
 826 [2013JA019388](https://doi.org/10.1002/2013JA019388) doi: <https://doi.org/10.1002/2013JA019388>
- 827 Jackman, C. M., Thomsen, M. F., & Dougherty, M. K. (2019). Survey of Sat-
 828 urn's magnetopause and bow shock positions over the entire Cassini mission:
 829 Boundary statistical properties and exploration of associated upstream condi-
 830 tions. *Journal of Geophysical Research: Space Physics*, 124(11), 8865-8883.
 831 Retrieved from [https://agupubs.onlinelibrary.wiley.com/doi/abs/](https://agupubs.onlinelibrary.wiley.com/doi/abs/10.1029/2019JA026628)
 832 [10.1029/2019JA026628](https://doi.org/10.1029/2019JA026628) doi: <https://doi.org/10.1029/2019JA026628>
- 833 Jackman, C. M., Thomsen, M. F., Mitchell, D. G., Sergis, N., Arridge, C. S.,
 834 Felici, M., ... Dougherty, M. K. (2015). Field dipolarization in Sat-
 835 urn's magnetotail with planetward ion flows and energetic particle flow
 836 bursts: Evidence of quasi-steady reconnection. *Journal of Geophysical*
 837 *Research: Space Physics*, 120(5), 3603-3617. Retrieved from [https://](https://agupubs.onlinelibrary.wiley.com/doi/abs/10.1002/2015JA020995)
 838 agupubs.onlinelibrary.wiley.com/doi/abs/10.1002/2015JA020995 doi:
 839 [10.1002/2015JA020995](https://doi.org/10.1002/2015JA020995)
- 840 Jasinski, J. M., Akhavan-Tafti, M., Sun, W., Slavin, J. A., Coates, A. J., Fuse-
 841 lier, S. A., ... Murphy, N. (2021). Flux transfer events at a reconnection-
 842 suppressed magnetopause: Cassini observations at Saturn. *Journal of*
 843 *Geophysical Research: Space Physics*, 126(2), e2020JA028786. Retrieved
 844 from [https://agupubs.onlinelibrary.wiley.com/doi/abs/10.1029/](https://agupubs.onlinelibrary.wiley.com/doi/abs/10.1029/2020JA028786)
 845 [2020JA028786](https://doi.org/10.1029/2020JA028786) (e2020JA028786 2020JA028786) doi: [https://doi.org/10.1029/](https://doi.org/10.1029/2020JA028786)
 846 [2020JA028786](https://doi.org/10.1029/2020JA028786)
- 847 Jasinski, J. M., Arridge, C. S., Bader, A., Smith, A. W., Felici, M., Kinrade, J., ...
 848 Murphy, N. (2019). Saturn's open-closed field line boundary: A Cassini
 849 electron survey at Saturn's magnetosphere. *Journal of Geophysical Re-*
 850 *search: Space Physics*, 124(12), 10018-10035. Retrieved from [https://](https://agupubs.onlinelibrary.wiley.com/doi/abs/10.1029/2019JA027090)
 851 agupubs.onlinelibrary.wiley.com/doi/abs/10.1029/2019JA027090 doi:
 852 <https://doi.org/10.1029/2019JA027090>
- 853 Jasinski, J. M., Slavin, J. A., Arridge, C. S., Poh, G., Jia, X., Sergis, N., ...
 854 Waite Jr., J. H. (2016). Flux transfer event observation at Saturn's day-
 855 side magnetopause by the Cassini spacecraft. *Geophysical Research Let-*
 856 *ters*, 43(13), 6713-6723. Retrieved from [https://agupubs.onlinelibrary](https://agupubs.onlinelibrary.wiley.com/doi/abs/10.1002/2016GL069260)
 857 [.wiley.com/doi/abs/10.1002/2016GL069260](https://doi.org/10.1002/2016GL069260) doi: [https://doi.org/10.1002/](https://doi.org/10.1002/2016GL069260)
 858 [2016GL069260](https://doi.org/10.1002/2016GL069260)
- 859 Jia, X., Hansen, K. C., Gombosi, T. I., Kivelson, M. G., Tóth, G., DeZeeuw,
 860 D. L., & Ridley, A. J. (2012). Magnetospheric configuration and dy-
 861 namics of Saturn's magnetosphere: A global MHD simulation. *Journal of*
 862 *Geophysical Research: Space Physics*, 117(A5). Retrieved from [https://](https://agupubs.onlinelibrary.wiley.com/doi/abs/10.1029/2012JA017575)
 863 agupubs.onlinelibrary.wiley.com/doi/abs/10.1029/2012JA017575 doi:
 864 <https://doi.org/10.1029/2012JA017575>
- 865 Johnson, J. R., Wing, S., & Delamere, P. A. (2014, 01). Kelvin Helmholtz insta-
 866 bility in planetary magnetospheres. *Space Science Reviews*, 184(1), 1-31. Re-
 867 trieved from <https://doi.org/10.1007/s11214-014-0085-z> doi: [10.1007/](https://doi.org/10.1007/s11214-014-0085-z)
 868 [s11214-014-0085-z](https://doi.org/10.1007/s11214-014-0085-z)
- 869 Jurac, S., & Richardson, J. D. (2005). A self-consistent model of plasma
 870 and neutrals at Saturn: Neutral cloud morphology. *Journal of Geo-*
 871 *physical Research: Space Physics*, 110(A9). Retrieved from [https://](https://agupubs.onlinelibrary.wiley.com/doi/abs/10.1029/2004JA010688)

- agupubs.onlinelibrary.wiley.com/doi/abs/10.1029/2004JA010635 doi:
https://doi.org/10.1029/2004JA010635
- Kellett, S., Bunce, E. J., Coates, A. J., & Cowley, S. W. H. (2009). Thickness of Saturn's ring current determined from north-south Cassini passes through the current layer. *Journal of Geophysical Research: Space Physics*, 114(A4). Retrieved from <https://agupubs.onlinelibrary.wiley.com/doi/abs/10.1029/2008JA013942> doi: <https://doi.org/10.1029/2008JA013942>
- Lapedes, A., & Farber, R. (1987). How neural nets work. In (p. 442-456). doi: 10.1142/9789814434102_0012
- Masters, A., Mitchell, D. G., Coates, A. J., & Dougherty, M. K. (2011). Saturn's low-latitude boundary layer: 1. properties and variability. *Journal of Geophysical Research: Space Physics*, 116(A6). Retrieved from <https://agupubs.onlinelibrary.wiley.com/doi/abs/10.1029/2010JA016421> doi: <https://doi.org/10.1029/2010JA016421>
- McAndrews, H., Thomsen, M., Arridge, C., Jackman, C., Wilson, R., Hendersson, M., ... Coates, M., A.J. and. Dougherty (2009). Plasma in Saturn's nightside magnetosphere and the implications for global circulation. *Planetary and Space Science*, 57(14), 1714-1722. Retrieved from <https://www.sciencedirect.com/science/article/pii/S0032063309000750> doi: <https://doi.org/10.1016/j.pss.2009.03.003>
- McAndrews, H. J., Owen, C. J., Thomsen, M. F., Lavraud, B., Coates, A. J., Dougherty, M. K., & Young, D. T. (2008). Evidence for reconnection at Saturn's magnetopause. *Journal of Geophysical Research: Space Physics*, 113(A4). Retrieved from <https://agupubs.onlinelibrary.wiley.com/doi/abs/10.1029/2007JA012581> doi: <https://doi.org/10.1029/2007JA012581>
- Milan, S. E., Provan, G., & Hubert, B. (2007). Magnetic flux transport in the Dungey cycle: A survey of dayside and nightside reconnection rates. *Journal of Geophysical Research: Space Physics*, 112(A1). Retrieved from <https://agupubs.onlinelibrary.wiley.com/doi/abs/10.1029/2006JA011642> doi: 10.1029/2006JA011642
- Milovanov, A. V., Zelenyi, L. M., & Zimbardo, G. (1996). Fractal structures and power law spectra in the distant Earth's magnetotail. *Journal of Geophysical Research: Space Physics*, 101(A9), 19903-19910. Retrieved from <https://agupubs.onlinelibrary.wiley.com/doi/abs/10.1029/96JA01562> doi: <https://doi.org/10.1029/96JA01562>
- Neupane, B. R., Delamere, P. A., Wilson, R. J., & Ma, X. (2019). Quantifying mass and magnetic flux transport in Saturn's magnetosphere. *Journal of Geophysical Research: Space Physics*, 124(3), 1916-1926. Retrieved from <https://agupubs.onlinelibrary.wiley.com/doi/abs/10.1029/2018JA026022> doi: <https://doi.org/10.1029/2018JA026022>
- Pontius Jr., D. H., & Hill, T. W. (2009). Plasma mass loading from the extended neutral gas torus of Enceladus as inferred from the observed plasma corotation lag. *Geophysical Research Letters*, 36(23). Retrieved from <https://agupubs.onlinelibrary.wiley.com/doi/abs/10.1029/2009GL041030> doi: <https://doi.org/10.1029/2009GL041030>
- Provan, G., Cowley, S. W. H., Bradley, T. J., Bunce, E. J., Hunt, G. J., & Dougherty, M. K. (2018). Planetary period oscillations in Saturn's magnetosphere: Cassini magnetic field observations over the northern summer solstice interval. *Journal of Geophysical Research: Space Physics*, 123(5), 3859-3899. Retrieved from <https://agupubs.onlinelibrary.wiley.com/doi/abs/10.1029/2018JA025237> doi: <https://doi.org/10.1029/2018JA025237>
- Reed, J. J., Jackman, C. M., Lamy, L., Kurth, W. S., & Whiter, D. K. (2018). Low-frequency extensions of the Saturn kilometric radiation as a proxy for magnetospheric dynamics. *Journal of Geophysical Research: Space Physics*, 123(1), 443-463. Retrieved from <https://agupubs.onlinelibrary.wiley.com/doi/>

- abs/10.1002/2017JA024499 doi: <https://doi.org/10.1002/2017JA024499>
- Richardson, I. G., Cowley, S. W. H., Hones Jr., E. W., & Bame, S. J. (1987).
Plasmoid-associated energetic ion bursts in the deep geomagnetic tail: Properties of plasmoids and the postplasmoid plasma sheet. *Journal of Geophysical Research: Space Physics*, 92(A9), 9997-10013. Retrieved from <https://agupubs.onlinelibrary.wiley.com/doi/abs/10.1029/JA092iA09p09997>
doi: <https://doi.org/10.1029/JA092iA09p09997>
- Russell, C. T., Jackman, C. M., Wei, H. Y., Bertucci, C., & Dougherty, M. K. (2008). Titan's influence on Saturnian substorm occurrence. *Geophysical Research Letters*, 35(12). Retrieved from <https://agupubs.onlinelibrary.wiley.com/doi/abs/10.1029/2008GL034080> doi: 10.1029/2008GL034080
- Schneider, S., Greenberg, S., Taylor, G. W., & Kremer, S. C. (2020). Three critical factors affecting automated image species recognition performance for camera traps. *Ecology and Evolution*, 10(7), 3503-3517. Retrieved from <https://onlinelibrary.wiley.com/doi/abs/10.1002/ece3.6147> doi: <https://doi.org/10.1002/ece3.6147>
- Sergis, N., Arridge, C. S., Krimigis, S. M., Mitchell, D. G., Rymer, A. M., Hamilton, D. C., ... Coates, A. J. (2011). Dynamics and seasonal variations in Saturn's magnetospheric plasma sheet, as measured by Cassini. *Journal of Geophysical Research: Space Physics*, 116(A4). Retrieved from <https://agupubs.onlinelibrary.wiley.com/doi/abs/10.1029/2010JA016180> doi: <https://doi.org/10.1029/2010JA016180>
- Slavin, J. A., Smith, E. J., Tsurutani, B. T., Sibeck, D. G., Singer, H. J., Baker, D. N., ... Scarf, F. L. (1984). Substorm associated traveling compression regions in the distant tail: Isee-3 Geotail observations. *Geophysical Research Letters*, 11(7), 657-660. Retrieved from <https://agupubs.onlinelibrary.wiley.com/doi/abs/10.1029/GL011i007p00657> doi: 10.1029/GL011i007p00657
- Smith, A. W., Jackman, C. M., Frohmaier, C. M., Fear, R. C., Slavin, J. A., & Coxon, J. C. (2018c). Evaluating single spacecraft observations of planetary magnetotails with simple Monte Carlo simulations: 2. magnetic flux rope signature selection effects. *Journal of Geophysical Research: Space Physics*, 123(12), 10,124-10,138. Retrieved from <https://agupubs.onlinelibrary.wiley.com/doi/abs/10.1029/2018JA025959> doi: <https://doi.org/10.1029/2018JA025959>
- Smith, A. W., Jackman, C. M., & Thomsen, M. F. (2016). Magnetic reconnection in Saturn's magnetotail: A comprehensive magnetic field survey. *Journal of Geophysical Research: Space Physics*, 121(4), 2984-3005. Retrieved from <https://agupubs.onlinelibrary.wiley.com/doi/abs/10.1002/2015JA022005> doi: 10.1002/2015JA022005
- Smith, A. W., Jackman, C. M., Thomsen, M. F., Lamy, L., & Sergis, N. (2018a). Multi-instrument investigation of the location of Saturn's magnetotail x-line. *Journal of Geophysical Research: Space Physics*, 123(7), 5494-5505. Retrieved from <https://agupubs.onlinelibrary.wiley.com/doi/abs/10.1029/2018JA025532> doi: 10.1029/2018JA025532
- Smith, A. W., Jackman, C. M., Thomsen, M. F., Sergis, N., Mitchell, D. G., & Roussos, E. (2018b). Dipolarization fronts with associated energized electrons in Saturn's magnetotail. *Journal of Geophysical Research: Space Physics*, 123(4), 2714-2735. Retrieved from <https://agupubs.onlinelibrary.wiley.com/doi/abs/10.1002/2017JA024904> doi: 10.1002/2017JA024904
- Smith, A. W., Slavin, J. A., Jackman, C. M., Fear, R. C., Poh, G.-K., DiBraccio, G. A., ... Trenchi, L. (2017). Automated force-free flux rope identification. *Journal of Geophysical Research: Space Physics*, 122(1), 780-791. Retrieved from <https://agupubs.onlinelibrary.wiley.com/doi/abs/10.1002/2016JA022994> doi: <https://doi.org/10.1002/2016JA022994>
- Staniland, N. R., Dougherty, M. K., Masters, A., & Bunce, E. J. (2020). De-

- termining the nominal thickness and variability of the magnetodisc current sheet at Saturn. *Journal of Geophysical Research: Space Physics*, 125(5), e2020JA027794. Retrieved from <https://agupubs.onlinelibrary.wiley.com/doi/abs/10.1029/2020JA027794> (e2020JA027794 10.1029/2020JA027794) doi: <https://doi.org/10.1029/2020JA027794>
- Szego, K., Nemeth, Z., Erdos, G., Foldy, L., Bebesi, Z., Thomsen, M., & Delapp, D. (2012). Location of the magnetodisk in the nightside outer magnetosphere of Saturn near equinox based on ion densities. *Journal of Geophysical Research: Space Physics*, 117(A9). Retrieved from <https://agupubs.onlinelibrary.wiley.com/doi/abs/10.1029/2012JA017817> doi: <https://doi.org/10.1029/2012JA017817>
- Thomsen, M. F., Jackman, C. M., Tokar, R. L., & Wilson, R. J. (2014). Plasma flows in Saturn's nightside magnetosphere. *Journal of Geophysical Research: Space Physics*, 119(6), 4521-4535. Retrieved from <https://agupubs.onlinelibrary.wiley.com/doi/abs/10.1002/2014JA019912> doi: <https://doi.org/10.1002/2014JA019912>
- Vasyliunas, V. M. (1983). Plasma distribution and flow. In A. J. Dessler (Ed.), *Physics of the Jovian Magnetosphere* (p. 395-453). Cambridge University Press. doi: 10.1017/CBO9780511564574.013
- Vogt, M. F., Connerney, J. E., DiBraccio, G. A., Wilson, R. J., Thomsen, M. F., Ebert, R. W., ... Bolton, S. J. (2020). Magnetotail reconnection at Jupiter: A survey of Juno magnetic field observations. *Journal of Geophysical Research: Space Physics*, 125(3), e2019JA027486. Retrieved from <https://agupubs.onlinelibrary.wiley.com/doi/abs/10.1029/2019JA027486> (e2019JA027486 2019JA027486) doi: <https://doi.org/10.1029/2019JA027486>
- Vogt, M. F., Kivelson, M. G., Khurana, K. K., Joy, S. P., & Walker, R. J. (2010). Reconnection and flows in the Jovian magnetotail as inferred from magnetometer observations. *Journal of Geophysical Research: Space Physics*, 115(A6). Retrieved from <https://agupubs.onlinelibrary.wiley.com/doi/abs/10.1029/2009JA015098> doi: <https://doi.org/10.1029/2009JA015098>
- Yao, Z. H., Grodent, D., Ray, L. C., Rae, I. J., Coates, A. J., Pu, Z. Y., ... Dunn, W. R. (2017). Two fundamentally different drivers of dipolarizations at Saturn. *Journal of Geophysical Research: Space Physics*, 122(4), 4348-4356. Retrieved from <https://agupubs.onlinelibrary.wiley.com/doi/abs/10.1002/2017JA024060> doi: 10.1002/2017JA024060
- Ying, X. (2019). An overview of overfitting and its solutions. In *Journal of physics: Conference series* (Vol. 1168, p. 022022).
- Zieger, B., Hansen, K. C., Gombosi, T. I., & De Zeeuw, D. L. (2010). Periodic plasma escape from the mass-loaded Kronian magnetosphere. *Journal of Geophysical Research: Space Physics*, 115(A8). Retrieved from <https://agupubs.onlinelibrary.wiley.com/doi/abs/10.1029/2009JA014951> doi: <https://doi.org/10.1029/2009JA014951>